DE-AC21-95MC32085--99

Screening of Candidate Corrosion Resistant Materials for Coal Combustion Environments - Volume IV

Final Report
January 31, 1997

By
Daniel E. Boss

Work Performed Under Contract No.: DE-AC21-95MC32085

For
U.S. Department of Energy
Office of Fossil Energy
Federal Energy Technology Center
P.O. Box 880
Morgantown, West Virginia 26507-0880

By
Northwestern University
BIRL
1801 Maple Avenue
Evanston, Illinois 60201-3135

Disclaimer

DISCLAIMER

Portions of this document may be illegible electronic image products. Images are produced from the best available original document.

ACKNOWLEDGMENT

I would like to thank John Hurley of UND-EERC for supplying the ash sample and his insight into the combustion environment. The technical input of Lee Paulson of METC and Dr. Helen Pickup, formerly of Hague International, was invaluable in understanding the application environment for the SiC heat exchanger tubes. I would like to thank Steve Wilhelm, Paul Rudnik, and Michael Wieczorek of BIRL for their support throughout the testing and analysis of these materials. Finally, I would like to thank Ted McMahon, the COR for this project at METC, for his support throughout this effort. The expertise and support of these, and other, colleagues contributed greatly to this effort.

TABLE OF CONTENTS

LIST OF TABLES

TABLE OF FIGURES

SCREENING OF CANDIDATE CORROSION RESISTANT MATERIALS FOR COAL COMBUSTION ENVIRONMENTS

1.0 EXECUTIVE SUMMARY

The development of a silicon carbide (SiC) heat exchanger is a critical step in the development of the Externally-Fired Combined Cycle (EFCC) power system. SiC is the only material that provides the necessary combination of resistance to creep, thermal shock, and oxidation. While the SiC structural materials provide the thermomechanical and thermophysical properties needed for an efficient system, the mechanical properties of the SiC tubes are severely degraded through corrosion by the coal combustion products. To obtain the necessary service life of thousands of hours at temperature, a protective coating is needed that is stable with both the SiC tube and the coal combustion products, resists erosion from the particle laden gas stream, is thermal-shock resistant, adheres to SiC during repeated thermal shocks (start-up, process upsets, shut-down), and allows the EFCC system to be cost competitive. The candidate protective materials identified in a previous effort were screened for their stability to the EFCC combustion environment. Bulk samples of each of the eleven candidate materials were prepared, and exposed to coal slag for 100 hours at 1370°C under flowing air. After exposure the samples were mounted, polished, and examined via x-ray diffraction, energy dispersive spectroscopy, and scanning electron microscopy. In general, the alumina-based materials behaved well, with comparable corrosion depths in all five samples. Magnesium chromite formed a series of reaction products with the slag, which included an alumina-rich region. These reaction products may act as a diffusion barrier to slow further reaction between the magnesium chromite and the slag and prove to be a protective coating. As for the other materials; calcium titanate failed catastrophically, the CS-50 exhibited extension microstructural and compositional changes, and zirconium titanate, barium zironate, and yttrium chromite all showed evidence of dissolution with the slag.

2.0 INTRODUCTION

The EFCC Program is intended to demonstrate a direct-coal combustion combined cycle power system[1,2]. To achieve power plant efficiencies in excess of 45 percent, high pressure air heaters, capable of driving modern gas turbines are necessary[2]. It is anticipated that an air temperature of at least 1100°C will be necessary, and that the exterior tube surface may see temperatures of 1370°C. The heat exchanger will be pressurized to 100 psi, and must provide a service life of thousands of hours at these thermomechanical loads and in a coal combustion gas stream. The developers of the EFCC system have evaluated a number of ceramic materials, including monolithic oxides, discontinuously reinforced composites, and continuous-fiber ceramic composites (CFCC). The preferred materials for the tubes are reaction-bonded silicon carbide (RBSiC) and sintered SiC, because of their creep and thermal shock resistance[3]. Another attractive feature of SiC is its hardness at elevated temperatures. It is expected that particles approximately 30 μm in diameter will be entrained in the gas stream and impact the tubes[3].

Numerous studies have shown that SiC is attacked by coal slag, and that its mechanical properties are significantly degraded by corrosion with time[4,5,6,7,8,9,10]. Other ceramics, such as

DuPont Lanxide's DiMOX™(SiC_p/Al_2O_3) hold up well to the corrosive environment[11,12], but do not have the necessary creep resistance at the operating temperature. Selection of a protective coating for SiC is difficult because of the narrow range of thermophysical properties (coefficient of thermal expansion match with SiC, high melting temperature, erosion resistance, high thermal shock resistance) and the highly complex thermochemical application environment. At 1370°C, most coal slags are molten, and the composition of the slag changes depending upon the source of the coal. Unfortunately, power plants do not run with coal from only one source. The University of North Dakota - Energy and Environmental Research Center (UND-EERC) has done extensive work on coal ash and its effect on ceramics. The factors influencing the corrosion of ceramics in coal-combustion environments were reviewed by Hurley[13], and UND-EERC has established a stockpile of ash samples to aide in establishing a common basis for materials evaluation.

In our previous work, we undertook a materials selection process which reviewed current literature and research efforts related to this problem, and complemented this effort with thermodynamic modeling and review of existing phase diagram information. After discussion with other researchers in this area, three classes of protective coatings were selected: 1) alumina-based materials, 2) materials stable with silica, and 3) materials with a low CTE. The goal was then to identify candidate materials that fit into each of these classes that also may be expected to provide the required balance of thermophysical properties, thermochemical stability, and lower processing costs. All of the candidate materials were reviewed for their strengths in the following categories: 1) chemical compatible with SiC; 2) stability in an oxidizing environment with the slag; and 3) potential for erosion resistance. The materials selection process led to the identification of eleven candidate materials for use in corrosion experiments. The candidate materials are summarized in Table 1 by their classification. A complete discussion of the materials and selection process is provided in a previous report*.

Table 1. Candidate Protective Materials

Alumina-Based	Silica Stable	Low Expansion Materials	Other
$3Al_2O_3•2SiO_2$	$BaZrO_3$	NZP (CS-50)	$CaTiO_3$
Al_2TiO_5/Al_2O_3	$MgCr_2O_4$	$ZrTiO_4$	
SiC_p/Al_20_3	$YCrO_3$	Al_2TiO_5	
		$3Al_2O_3•2SiO_2$ / Al_2TiO_5	

Notes: NZP = sodium zirconium phosphate - type material; CS-50 = calcium strontium variation of NZP supplied by LoTec

The goal of this work was to evaluate both the corrosion and potential erosion resistance of the candidate materials identified in our previous effort. The potential erosion resistance of the

* D. Boss, "Corrosion Resistant Coatings For Silicon Carbide Heat Exchangers" DOE contract #DE-AC21-95MC32085

materials was to be evaluated via hot hardness measurement. It is our belief that the hardness and toughness information from these tests would provide insight into their erosion resistance. Unfortunately, we were not able to perform the hot-hardness measurements within the scope of this current project. The materials listed in Table 1, as well as baseline SiC and Al_2O_3 materials, were exposed to coal slag 1370°C for 100 hours.

3.0 EXPERIMENTAL PROCEDURE

3.1 - Sample Preparation

The ash sample used for all corrosion testing was from an Illinois #6 coal fired in the Baldwin Plant, supplied by UND-EERC, with the composition shown in Table 2. This ash was collected from a cyclone combustor with a firing temperature over 1300°C. These firing conditions are representative of those expected for an EFCC system. A key factor in the selection of this ash was the absence of sodium, since it is not expected to be present in the slag that collects on the EFCC heat exchanger tubes.

Table 2. Chemical Composition of Baldwin Slag

Oxide (weight percent)	Baldwin Slag
SiO_2	53.4
Al_2O_3	18.6
Fe_2O_3	17.6
TiO_2	0.7
P_2O_5	0.0
CaO	7.1
MgO	0.9
Na_2O	0.0
K_2O	1.7
SO_3	0.0

Whenever possible, bulk samples of the candidate materials were obtained from commercial sources. Powders for processing of other samples were also purchased when possible. Synthesis of powders was necessary for only the $MgCr_2O_4$ and $YCrO_3$ samples. A summary of the processing conditions for all samples is presented in Table 3.

Table 3. Materials Preparation Summary

Material	Sample Preparation[1]
SiC (RBSiC, sintered)	supplied by Carborundum as dense plates
Al_2O_3	supplied by Coors as dense rods
$3Al_2O_3 \cdot 2SiO_2$	Powder supplied by Baikowski (Baikalox lot#2126), sintered at 1650°C for 2 hours in air
Al_2TiO_5/Al_2O_3	Al2TiO5 supplied by F. J. Brodman (Flowmaster lot #47595), alumina supplied by Baikowski (Baikalox lot #437m); sintered at 1500°C for 2 hours in air
SiC_p/Al_2O_3	Al supplied by Fischer (#A550-500), SiC particulate supplied by Superior Graphite (HSC Grade 059s), alumina supplied by Baikowski (Baikalox lot #437m); prepared by reaction bonding after Wu[14], sintered in three steps; at 1550°C for 1 hours in air, at 1600°C for 2 hours in air, and at 1700°C for 4 hours in air
$BaZrO_3$	Aldrich #38,330-9 (<10 μm), sintered at 1600°C for 1.5 hrs in air
$MgCr_2O_4$	powder prepared by combustion synthesis[15] using $Cr(NO_3)_3 \cdot 9H_2O$ Aldrich #23,925-9, $Mg(NO_3)_2 \cdot 6H_2O$ Aldrich #23,717-5, and urea Aldrich #20,888-4, and then sintered at 1800°C for 2 hours (inert)
$YCrO_3$	powder prepared by precipitation from nitrates ($Y(NO_3)_3 \cdot 5H_2O$ Aldrich #23,795-7, $Cr(NO_3)_3 \cdot 9H_2O$ Aldrich #23,925-9), calcined at 1100°C, sintered at 1800°C (inert) for 2 hours
NZP (CS-50)	supplied by LoTec as dense rods
$ZrTiO_4$	Alfa #39490 (<10 μm), sintered at 1600°C for 1.5 hours in air
Al_2TiO_5	supplied by F. J. Brodmann as dense blocks
$3Al_2O_3 \cdot 2SiO_2$ / Al_2TiO_5	mullite supplied by Baikowski (Baikalox lot#2126), Al2TiO5 supplied by F. J. Brodman (Flowmaster #47595), sintered at 1500°C for 2 hours in air
$CaTiO_3$	powder purchased from Aldrich (#37,260-9), sintered at 1500°C for 1.5 hours in air

Note: [1] All sintered samples were mixed with 1 w/o Butvar 76 binder, uniaxially pressed to 6 ksi, and then cold-isostatically pressed at 40 ksi.

3.2 - Corrosion Experiments

The exposure conditions suggested by Hague and UND-EERC for initial screening of materials consisted of an Eastern coal ash, flowing air, and a sample temperature of approximately 1370°C. A molybdenum disilicide furnace (Deltech Model #DT-31) with a programmable temperature controller was configured with an alumina closed-one end tube (Vesuvius McDanel #998A-3125-24-COE) as a retort. A schematic of the system is shown in Figure 1. The alumina retort has an outer diameter of 3 inches, an inner diameter of 2.5 inches, and a length of 24 inches. The open end of the retort was fitted with a flange for atmosphere control. Each sample was placed in an individual alumina crucible (Johnson Matthey #32952 - 20 ml) which was then half-filled with ash provided by UND-EERC. The bottom of the retort was fitted with alumina insulating block to provide a stable support for the crucibles and to center the crucibles in the furnace hot-zone. Using this configuration, three crucibles could be placed inside the retort

simultaneously. A 100 sccm flow of clean, dry air was feed into the retort to provide a continuous feed of oxygen into the retort. The dry air was run through a bubbler filled with deionized water at ambient temperature to provide a consistent moisture level. The air flow was controlled using a commercial mass flow control system (MKS). With the samples inside a retort, a temperature calibration run was made to determine that a furnace temperature of 1510°C was necessary to obtain a sample temperature of approximately 1370°C. Experimental parameters for the exposure tests, such as temperature versus time, air flow, and ambient temperature, were collected by a data acquisition system for later analysis.

3.3 - Sample Analysis

After exposure to the ash for 100 hours at 1370°C, macrophotos of the samples in their crucibles were taken to document the gross effect of the ash on the materials. Each material was then removed from the crucible, sectioned with a water cooled diamond saw, and metallographically prepared. Each sample was vacuum encapsulated in epoxy, and polished to a 3 μm diamond finish. X-ray diffraction was performed on the baseline and exposed samples for selected materials using a Scintag XDS 2000 diffractometer and $Cu_{k\alpha}$ radiation. For microanalysis, the metallographic samples were coated with carbon by evaporation (Bio-Rad E6100). Scanning electron microscopy (SEM) was performed using a JEOL JXA-840 microanalyzer equipped with a Tracor Northern 5600 Microscan energy dispersive spectroscopy (EDS) unit. On selected samples, standardless semi-quantitative (SSQ) analysis was done using the EDS system, which can produce composition analysis accurate to ±5 percent.

4.0 RESULTS AND DISCUSSION

The analytical results and discussion will be presented by material. The XRD patterns for all samples are provided for reference in Appendix A. For many samples, the as-fabricated and exposed XRD patterns have been placed on the same plot with the intensity of each pattern arbitrarily set at 1000 counts per second (cps). One of the patterns is displayed from 0 to 1000 cps, while the other is displayed from 1000 to 2000 cps. In cases where the plot is entitled "Exposed", the pattern for the sample after slag exposure is on the bottom. In many cases, little significant change is seen in the samples. When appropriate, a discussion of the XRD patterns for a specific material will be presented.

Silicon Carbide - SiC

Both the Hexalloy and RBSiC appeared to be relatively stable in the slag after exposure (Figure 2), although both were readily wet by the slag. Comparison of the XRD spectra before and after exposure for each sample showed that the residual free Si in the RBSiC had been greatly reduced, while no significant changes were detected in the Hexalloy sample. The SEM/EDS analysis of the Hexalloy sample was typical for both these materials. The slag-SiC interface (Figure 3) revealed etch pits, Si-Ca rich regions, Fe-Si precipitates, and Fe-rich regions typical of this sample. In Figure 3, the SiC is shown in the upper section of the micrograph, with the large porosity present in the slag. These type of slag-SiC interactions have been documented by others[5,9], and have been cited as the reduction of strength in SiC heat exchanger tubes.

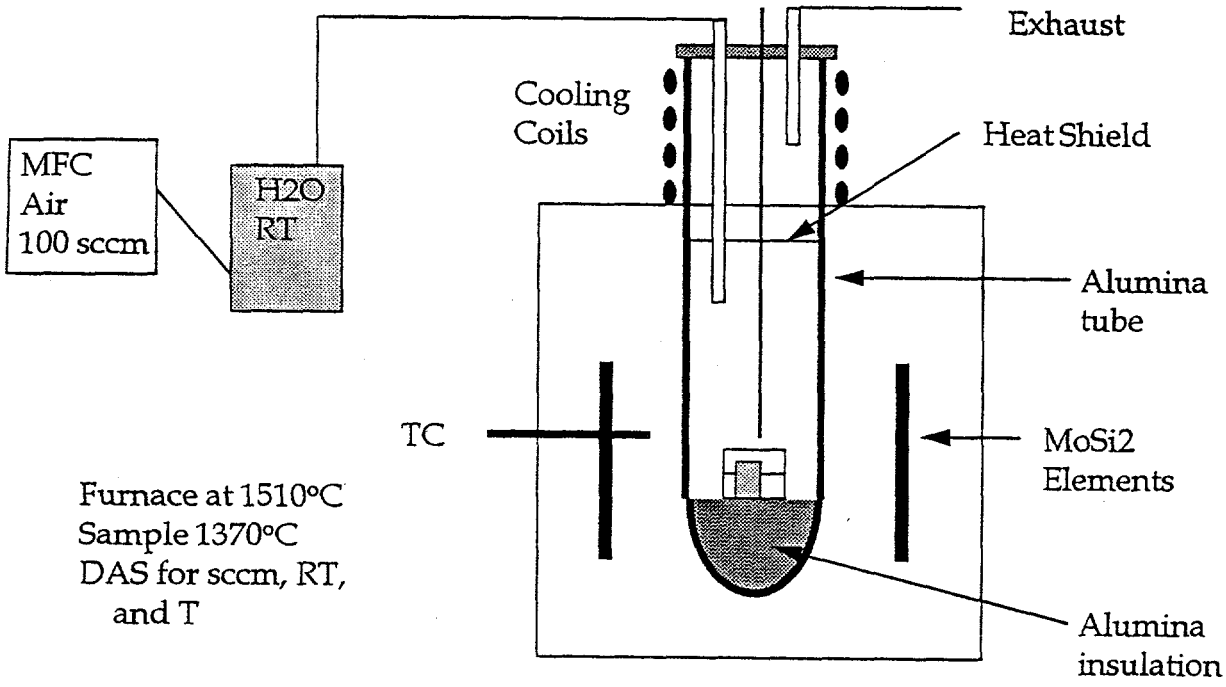

Figure 1. Experimental System

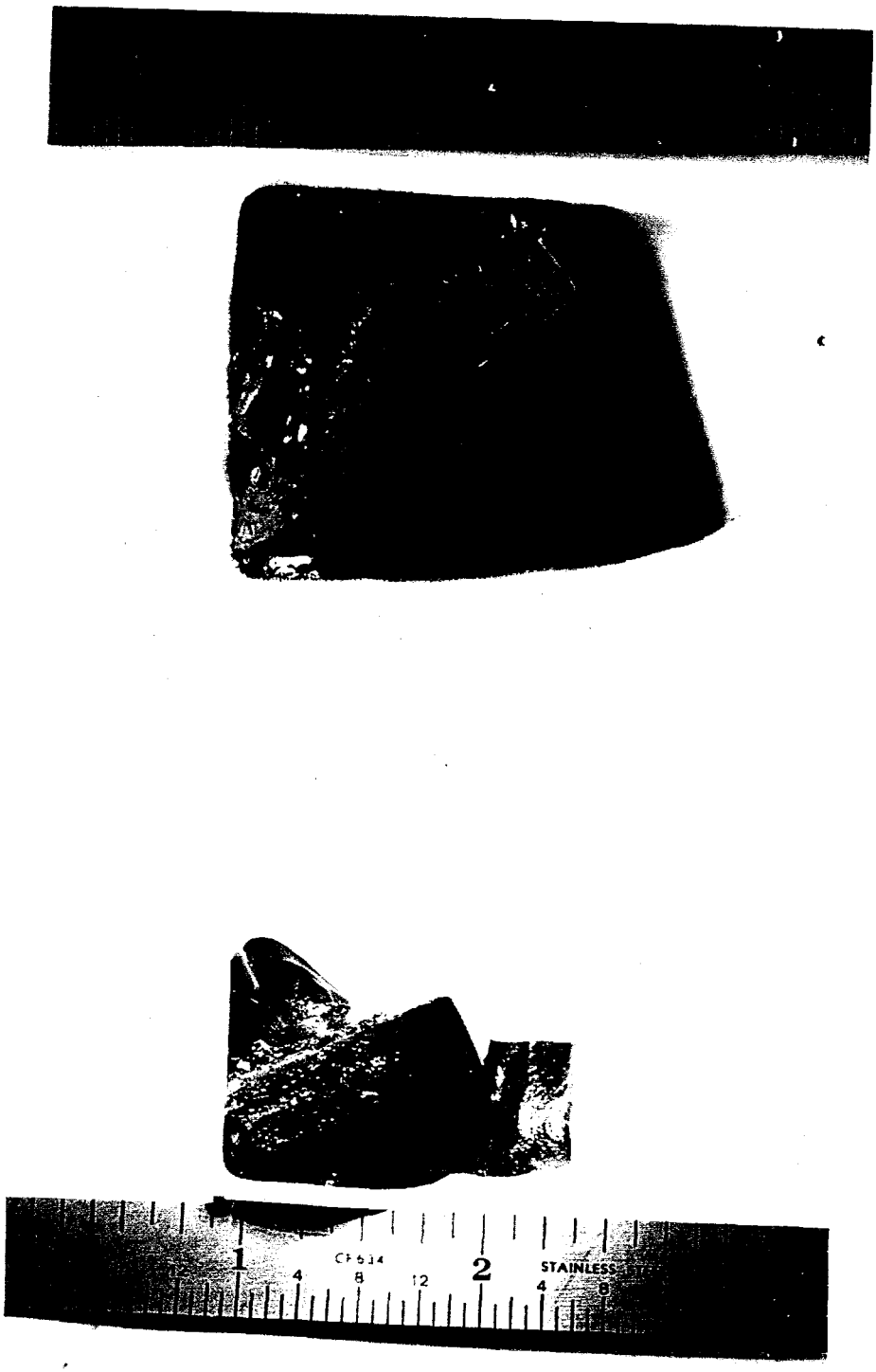

Figure 2. Macrophotos of Hexalloy (a, top) and RBSiC (b, bottom) after Exposure

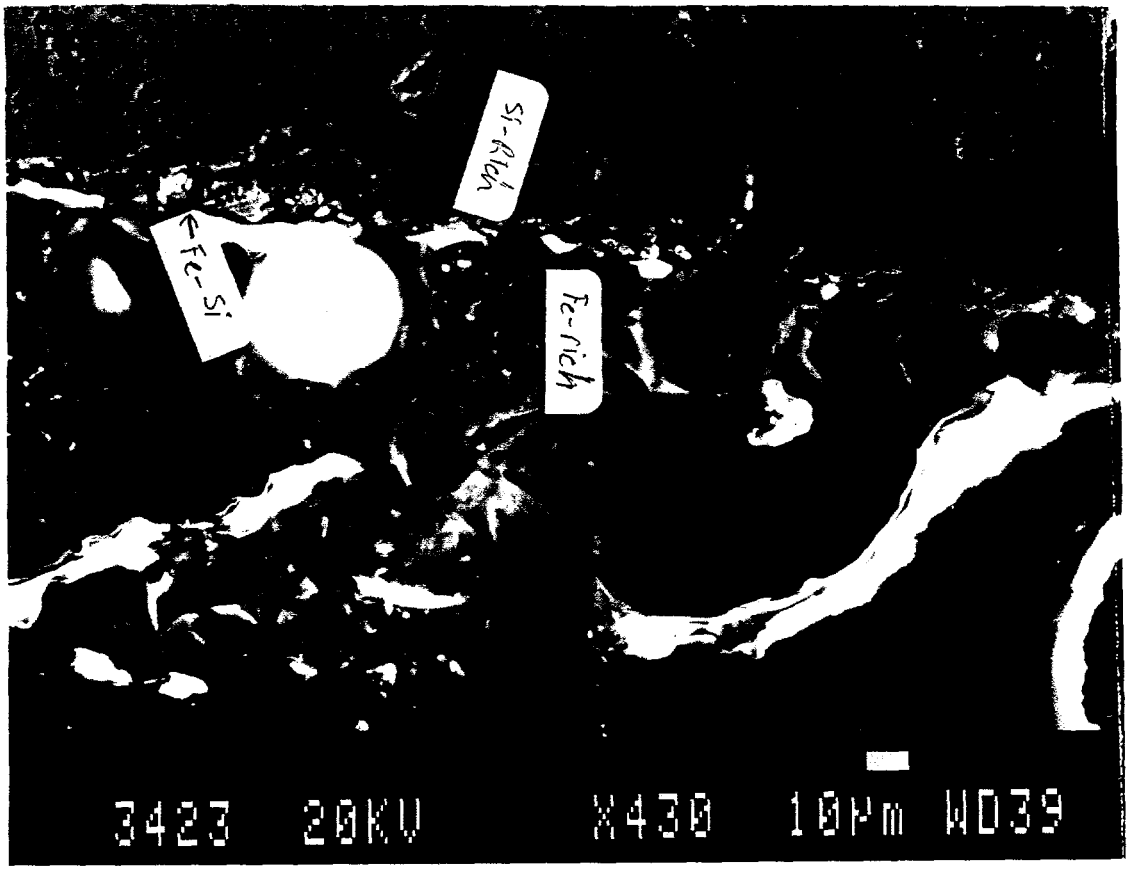

Figure 3. Hexalloy - Slag Interface After Exposure

Alumina - Al_2O_3

Alumina was included as a baseline material in this program because of its demonstrated stability in the coal slag environment. The alumina sample after exposure is shown in Figure 4. Though it was completely wet by the slag during exposure, it appears to have retained excellent dimensional stability. XRD analysis revealed no changes in the bulk structure of the alumina sample. Examination of the slag-Al_2O_3 interface via SEM showed a very clean phase boundary (Figure 5), with no apparent ingress of slag. A higher magnification view of the interface is shown in Figure 6 (alumina is on the left side) which verified the stability of Al_2O_3 in this slag. EDS examination of the alumina adjacent to the interface found only a slight (<5% intensity) increase for Si and Fe within 20 microns of the slag interface. No significant change in composition was found in the slag at the boundary.

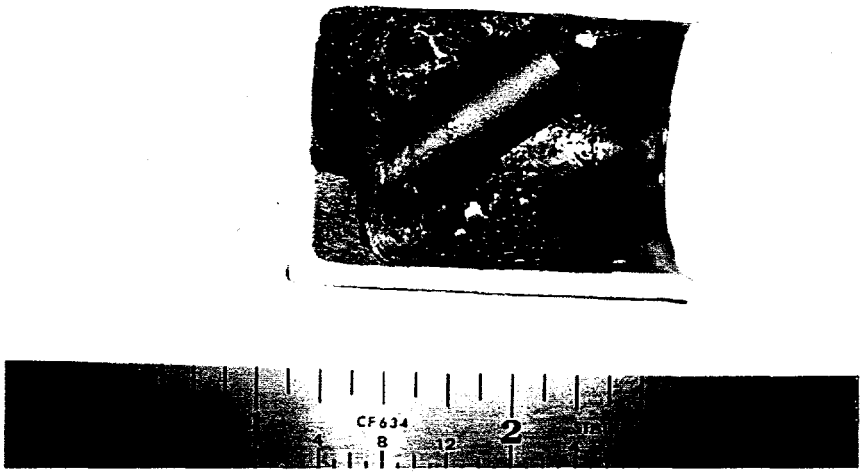

Figure 4. Alumina Sample After Slag Exposure

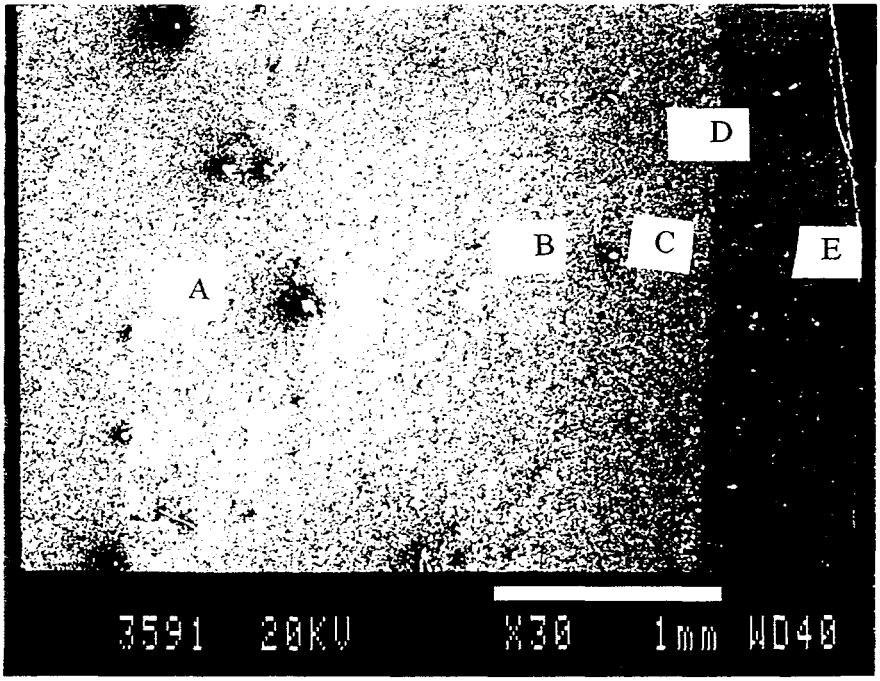

Figure 5. Overview of Alumina-Slag Interface After Exposure

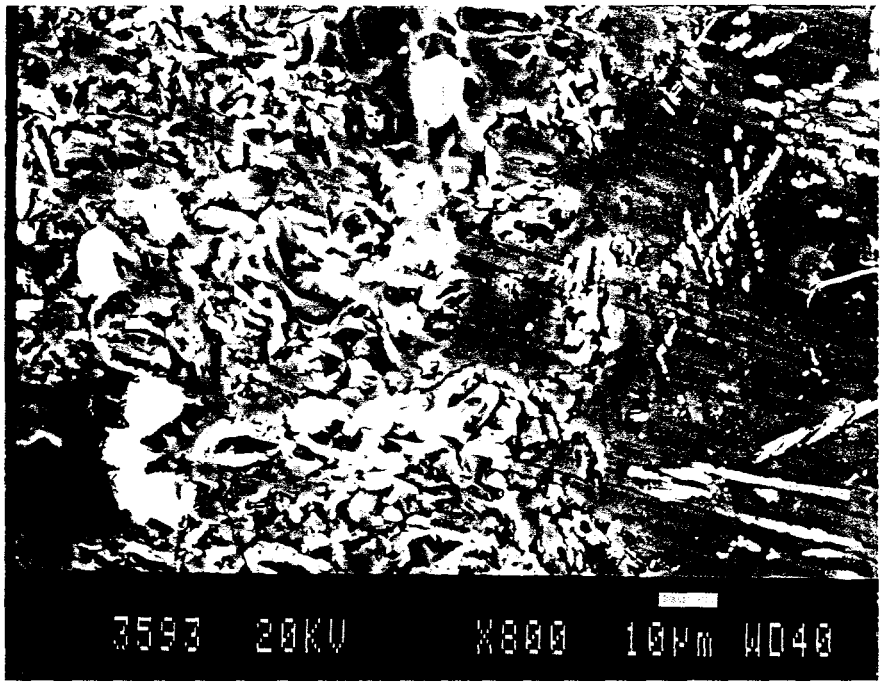

Figure 6. High Magnification View of Alumina-Slag Interface

Calcium Titanate - $CaTiO_3$

Calcium titanate has been used successfully as a corrosion resistant coating at intermediate temperatures, and this was one of the drivers for its selection. However, it was immediately apparent that this application environment was to severe for this material. Examination of the retort with this sample showed a catastrophic reaction between the slag, calcium titanate, and the small alumina crucible. The reaction was so severe (Figure 7) that it resulted in a complete failure of the bottom of the crucible, attack of the alumina insulation, and degradation of the alumina muffle tube holding the samples. The failure of this sample necessitated the replacement of the muffle tube, since the $CaTiO_3$ sample could not be removed without destroying it.

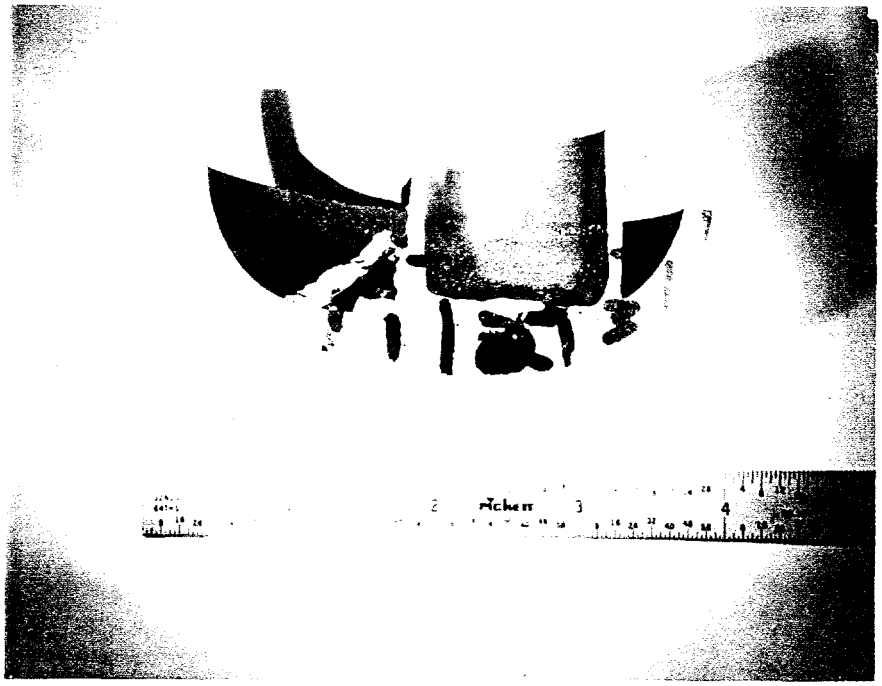

Figure 7. Failure of $CaTiO_3$ Samples

Mullite - $3Al_2O_3 \cdot 2SiO_2$

Mullite has been identified by a number of researchers as an attractive protective coating for SiC in coal combustion applications because of its CTE match with SiC and its high thermochemical stability to both acidic and basic slags. After exposure to the slag, the mullite sample had a thin coating on all surfaces, but seemed to retain its original dimensions without evidence of bloating or distortion (Figure 8). Examining the XRD patterns showed only that the peaks became sharper after exposure, with no obvious indication of reaction products. The results of the EDS examination of the mullite-slag interface (Figure 9) are summarized in Table 4. As can be seen by comparing the regions that were examined with the intensity profiles, the mullite sample was stable at areas A and B, with some minor introduction of calcium and iron species at area C. At D, a transition begins to occur which shows an enrichment of silicon, as well as calcium, potassium and iron species. At location E, the composition of the sample corresponds to that of the slag. Closer examination of the mullite-slag boundary did not show evidence of reaction products.

Table 4. Intensity of Detected Elements in Mullite Sample After Exposure

Intensity					
Area	**Al**	**Si**	**Ca**	**K**	**Fe**
A	.84	.25	.00	.00	.00
B	.75	.29	.00	.00	.03
C	.75	.31	.02	.00	.05
D	.68	.36	.03	.02	.05
E	.26	.60	.09	.04	.09

Figure 8. Mullite Sample After Exposure

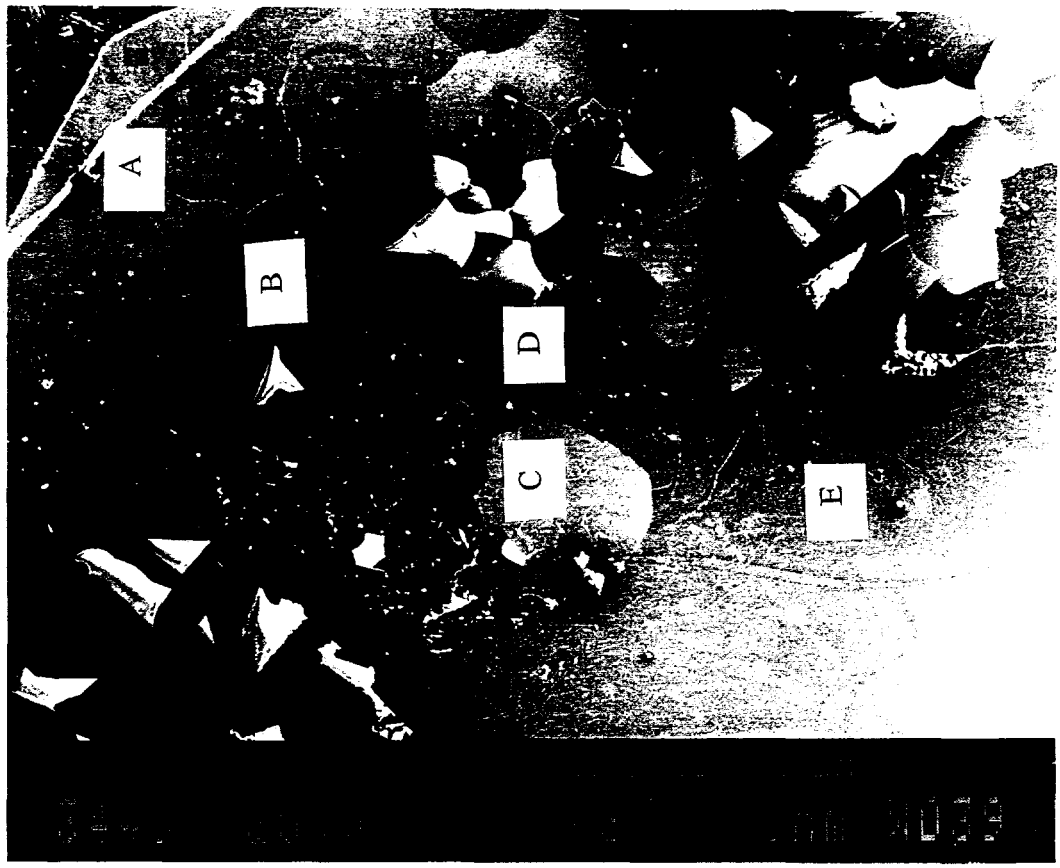

Figure 9. Mullite - Slag Boundary With Analysis Locations

Reaction Bonded Aluminum Oxide - RBAO (SiC_p/Al_2O_3)

In previous work on heat exchanger tubes[3], the DiMOX™ SiC_p/Al_2O_3 composites produced by DuPont Lanxide Composites demonstrated excellent thermochemical stability. However, these tubes did not possess sufficient creep strength. It would be attractive to deposit this type of material as a coating on SiC tubes, however, and the work by Wu and Claussen[15] with RBAO may present a means to accomplish this. Thus, RBAO was included in this effort. After consolidation of the RBAO, XRD analysis showed the presence of SiC, α-Al_2O_3, and several peaks corresponding to mullite. After exposure to the slag, the mullite had become the major phase with SiC and α-Al_2O_3 still present in substantial amounts. Visual examination of the RBAO after exposure showed that the slag had wet the entire sample. Examining the sample in cross-section (Figure 10) revealed a thick white oxide layer at the surface of the RBAO sample. The two locations where the oxide layer penetrates sharply into the bulk of the sample were probably caused by cracking of the sample during initial consolidation. The RBAO - slag boundary is shown in Figure 11, with the slag being on the right-hand side of the micrograph (Areas A and B). EDS analysis was performed at each of the indicated areas on the sample, with the results summarized in Table 5. Areas A and B were indicative of the bulk slag composition, with Area B located within 20 μm of the RBAO boundary. Area C, a region within 50 μm of the

slag boundary, showed only a small amount of Fe present in addition to the expected Al and Si. The transition in composition between Areas B and C appeared to be distinct with no apparent reaction products at the interface. Areas further away from the RBAO - slag boundary consistently showed predominately Al and Si, with only very minor amounts of Ca and/or Fe. As a comparison, a point in the center of the RBAO sample was examined (not shown in Figure 11) which showed Al and Si intensities of approximately 0.7 and 0.5, respectively. While the Al intensity in the center of the sample is consistent with Areas C - E, the exterior of the RBAO appears to contain less Si. The reason for this has not been determined, but it could be produced by a reaction with the slag, poor blending of the RBAO precursors, or sublimation of Si-based species during initial consolidation at temperatures up to 1700°C.

Table 5. Summary of EDS Analysis on RBAO-Slag Boundary

Area	Al	Si	Ca	K	Fe
A	.21	.59	.09	.04	.03
B	.25	.60	.09	.03	.05
C	.71	.22	.00	.00	.04
D	.70	.25	.02	.00	.03
E	.71	.30	.02	.00	.03
Center	.72	.50	.00	.00	.00

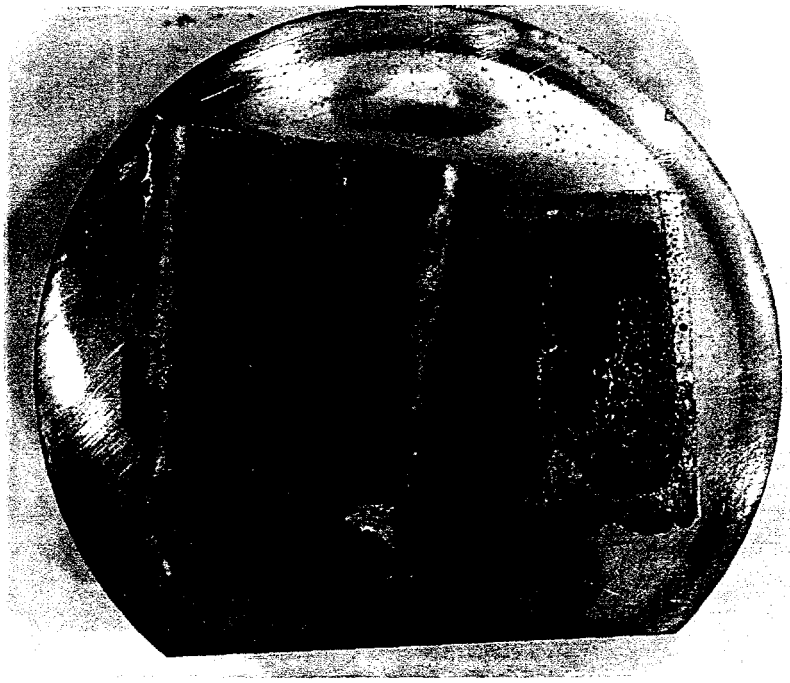

Figure 10. Cross-Section of RBAO Sample After Exposure

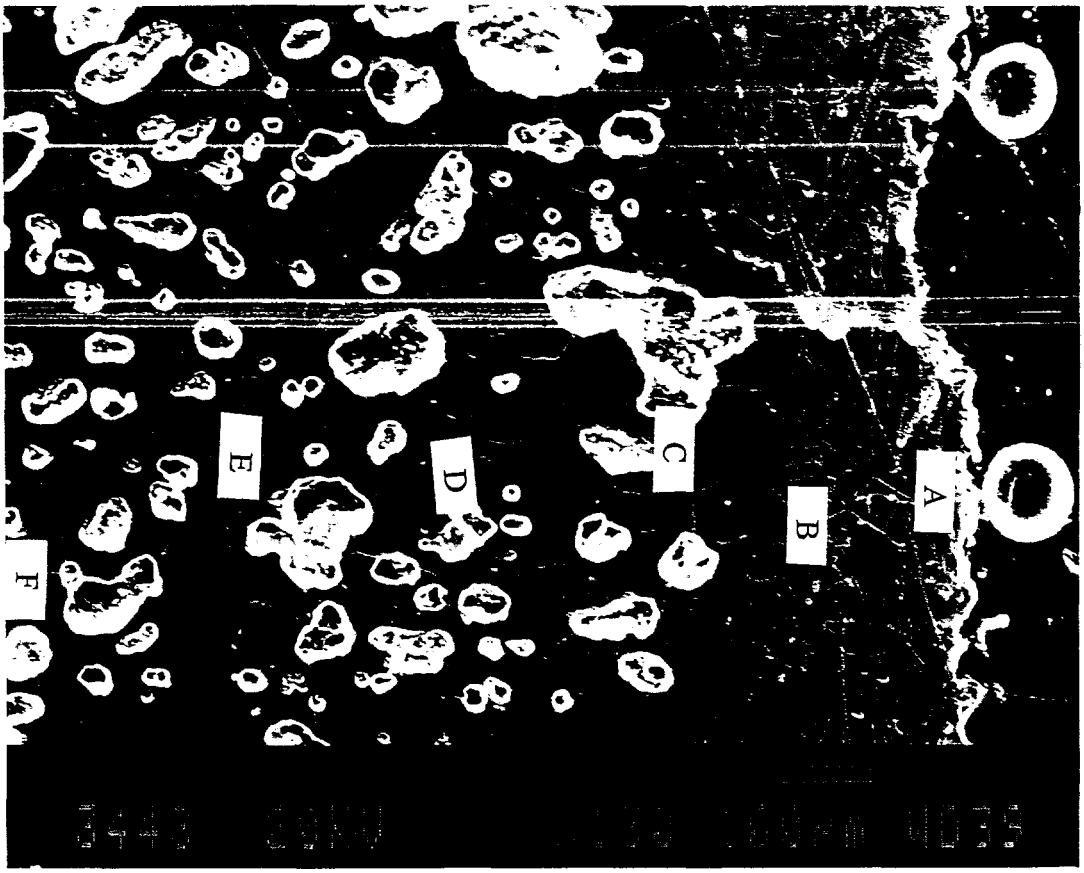

Figure 11. RBAO - Slag Boundary Showing Areas Examined by EDS

Aluminum Titanate - Al_2TiO_5

Aluminum titanate provides a good CTE match with SiC and it has been identified by other researchers[8,16] as a promising candidate for coal combustion environments. Two samples were run of the Al_2TiO_5 because the first sample fell completely into the slag (Figure 12) during exposure. The second sample remained upright (Figure 13). The XRD pattern for Al_2TiO_5 did not show any compositional change after exposure, and only exhibited an increase in peak intensity and definition. The results of the examination of slag boundary for Sample #1 via SEM (Figure 14) and EDS (Table 6) did show some change in the Al_2TiO_5. The EDS results for Area A show only Al and Ti present in the interior of the sample. In Area B, approximately 50 μm from the slag boundary, a significant level of Si and a trace amount of Fe all becoming enriched while the relative amount of Ti decreases. In the slag adjacent to the boundary, Al is enriched well above that found in the base slag (Area E). These results indicate some interaction between the Al_2TiO_5 and the slag, with the likely result of producing some substitution of Fe for Ti in the titanate structure, preferential removing of Al to enrich the slag, and possible the formation of Al-Si-O phases. The apparent extent of modification for the sample in the exposure time was on the order of 50 μm to 100 μm.

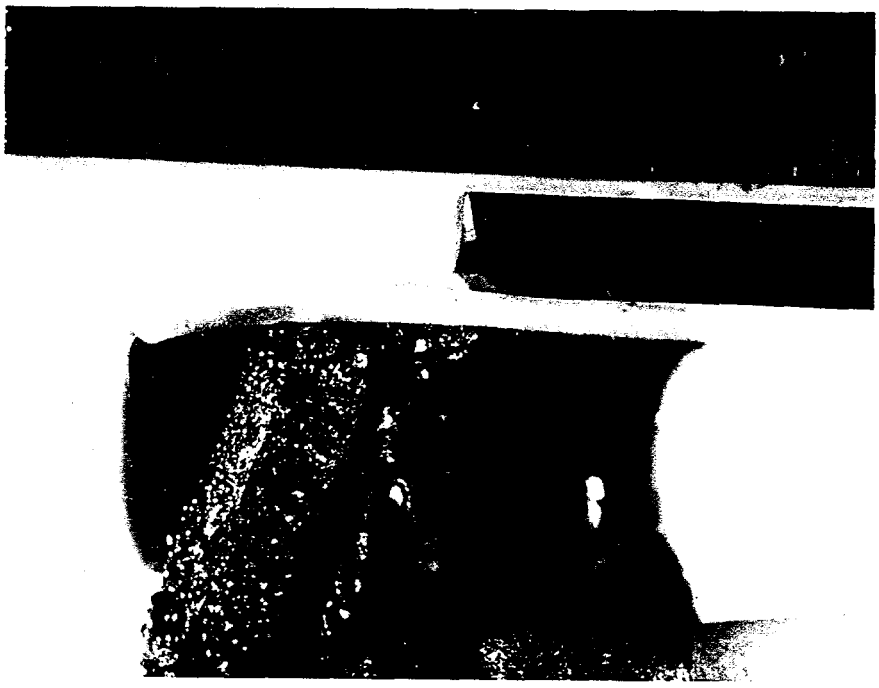

Figure 12. Al_2TiO_5 Sample #1 After Exposure

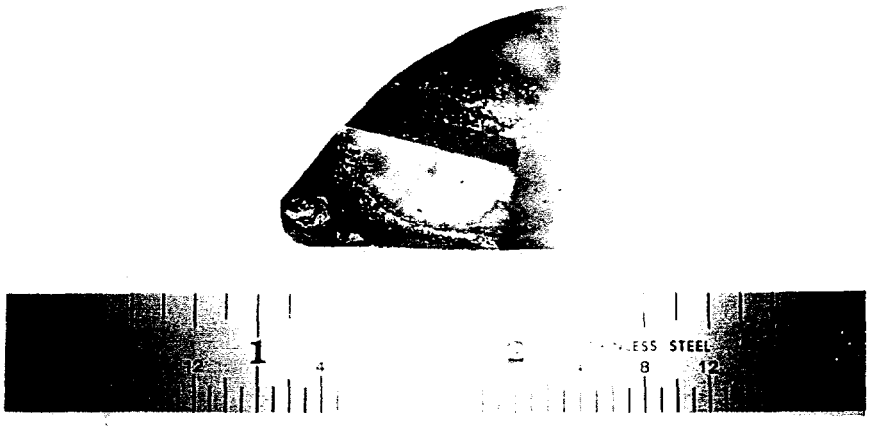

Figure 13. Al_2TiO_5 Sample #2 After Exposure

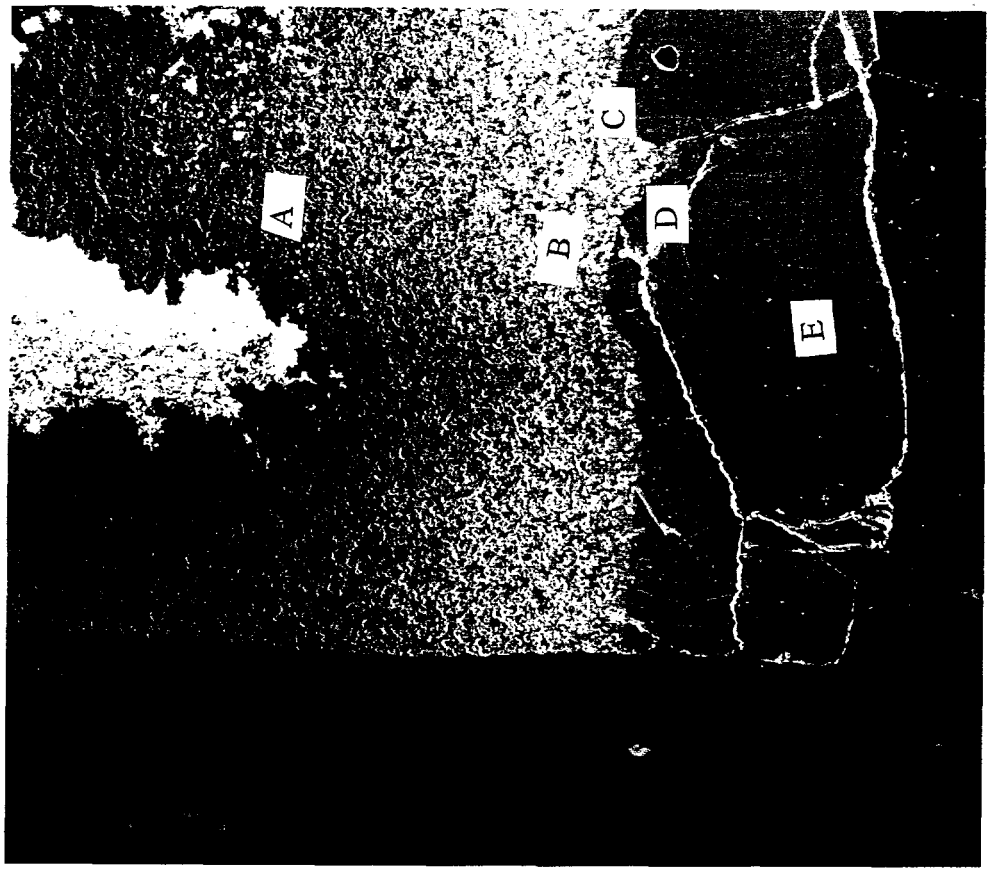

Figure 14. Al_2TiO_5 #1 - Slag Boundary

Table 6. EDS Analysis of Al_2TiO_5 Sample #1

Intensity (Sample 1)						
Area	**Al**	**Ti**	**Si**	**Fe**	**Ca**	**K**
A	.75	.63	.00	.00	.00	.00
B	.56	.31	.06	.03	.00	.00
C	.88	.50	.13	.15	.00	.00
D	.91	.08	.69	.15	.06	.04
E	.50	.05	.94	.16	.16	.06

In Sample #2, examination of the Al_2TiO_5 - slag boundary via SEM (Figure 15) apparently shows some differences in the slag adjacent to the sample. This boundary layer is darker and seems to exclude the bright precipitates typical of the bulk slag. The areas examined on the samples are shown in Figure 16, with the EDS results listed in Table 7. In the interior of the sample (Areas A and B), the Al to Ti ratio is consistent with the base material, and the small amount of Si shown could be contamination from the polishing process or a true indication of a small amount of Si in the material. In Areas C and D, Fe and Si appear to be present (300 μm to 500 μm from the surface of the sample), although they are both at very low levels. Area E shows strong evidence of Al_2TiO_5 interaction with Fe, while Area F shows both Si and Fe present and a

relative depletion of Ti. Inspection of Area G (the slag adjacent to the Al_2TiO_5) reveals a distinct compositional difference from the typical slag material (Area H). Area G is enriched in Al with little Ti and no Ca present. This would indicate that Al_2TiO_5 is undergoing some reaction with the slag. Possible reactions could be exchange of Fe for Al in the titanate structure, or a dissolution of the material. The results of the two Al_2TiO_5 samples are comparable, with both showing the ingress of Fe and Si into the Al_2TiO_5, and a modification of the slag composition near the sample surface.

Table 7. EDS Analysis of Al_2TiO_5 Sample #2

Intensity (Sample 2)						
Area	**Al**	**Ti**	**Si**	**Ca**	**K**	**Fe**
A	.80	.50	.06	.00	.00	.00
B	.75	.43	.04	.00	.00	.00
C	.80	.43	.04	.00	.00	.00
D	.75	.43	.04	.00	.00	.00
E	.67	.40	.04	.02	.00	.13
F	.63	.27	.10	.03	.00	.13
G	.54	.02	.16	.00	.00	.04
H	.40	.06	.88	.13	.05	.10

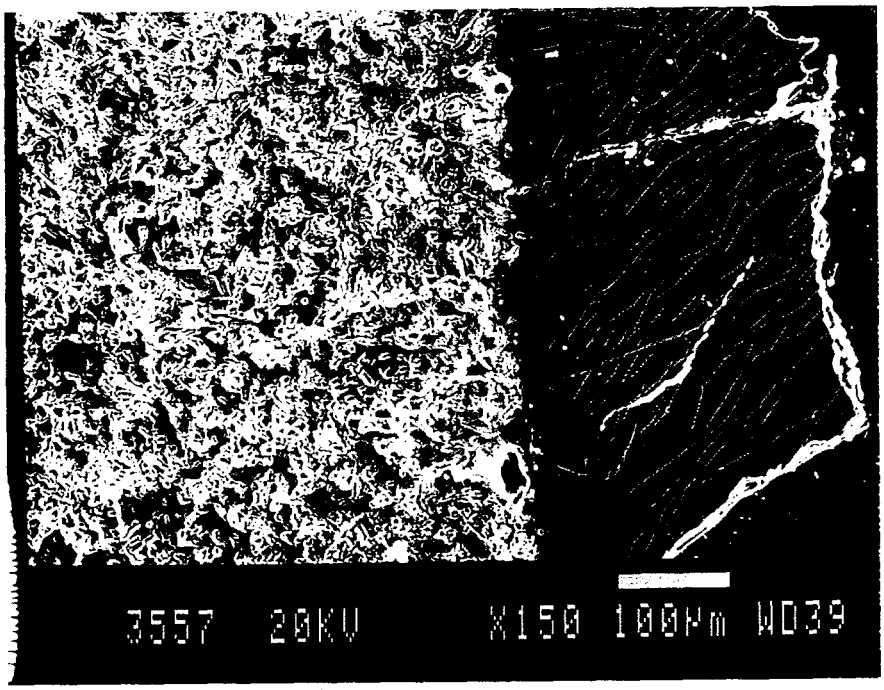

Figure 15. Al_2TiO_5 - Slag Boundary - 150X

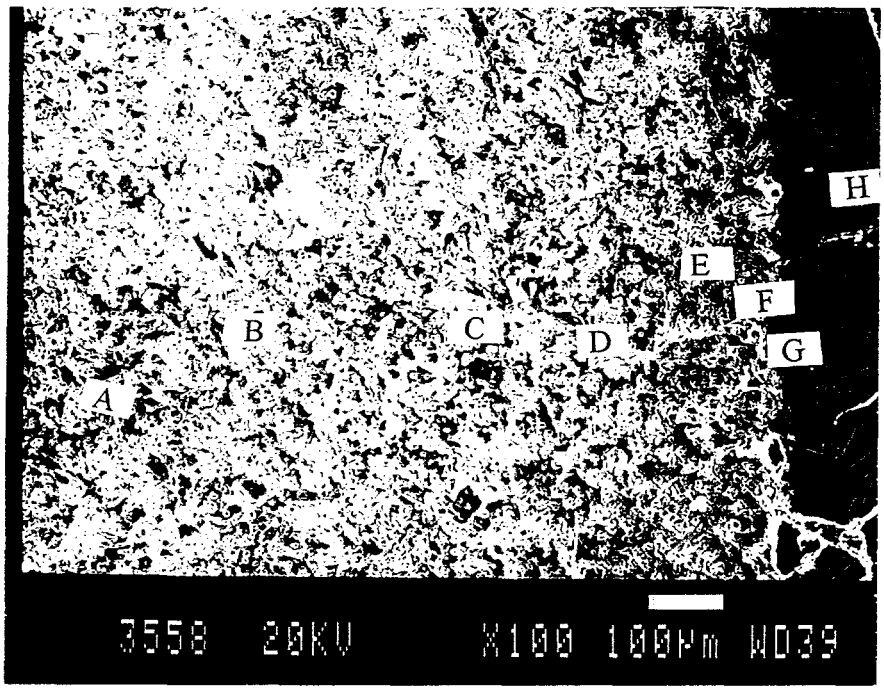

Figure 16. Analysis Locations on Al_2TiO_5 #2 Sample

Mullite/Aluminum Titanate - $3Al_2O_3 \cdot 2SiO_2/Al_2TiO_5$

One of the concerns with using Al_2TiO_5 is the potential for grain growth at the expected operating temperatures for the heat exchanger, which, because of the highly anisotropic CTE of Al_2TiO_5, would lead to spontaneous cracking of the material. Lin *et al.*[17] investigated a composite material consisting of approximately 10 weight percent mullite in an Al_2TiO_5 matrix. The mullite is thermodynamically stable with the Al_2TiO_5 and inhibits grain growth. The composite sample after exposure is shown in Figure 17. The sample may have been preferentially attacked at the melt line, and several circumferential cracks are evident in the sample The cracks are likely the result of defects introduced during green-body processing of the sample. Figure 18 shows an overview of the slag boundary area and the locations where EDS baseline material with only trace amounts of Ca, K, and Fe. At Area C, a region within 20 µm of the slag interface, Fe has diffused into the sample, but no morphological changes were noted. An abrupt transitions is made in composition in Area D, with the composition being typical of bulk slag (Area F). An unusual feature of this sample is the apparent change in composition in Area E, which is enriched in Al over either Areas D or F.

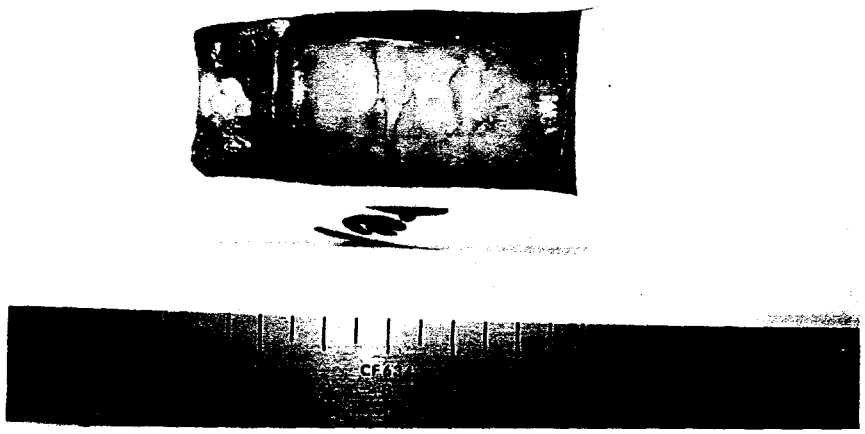

Figure 17. Mullite/Aluminum Titanate After Exposure

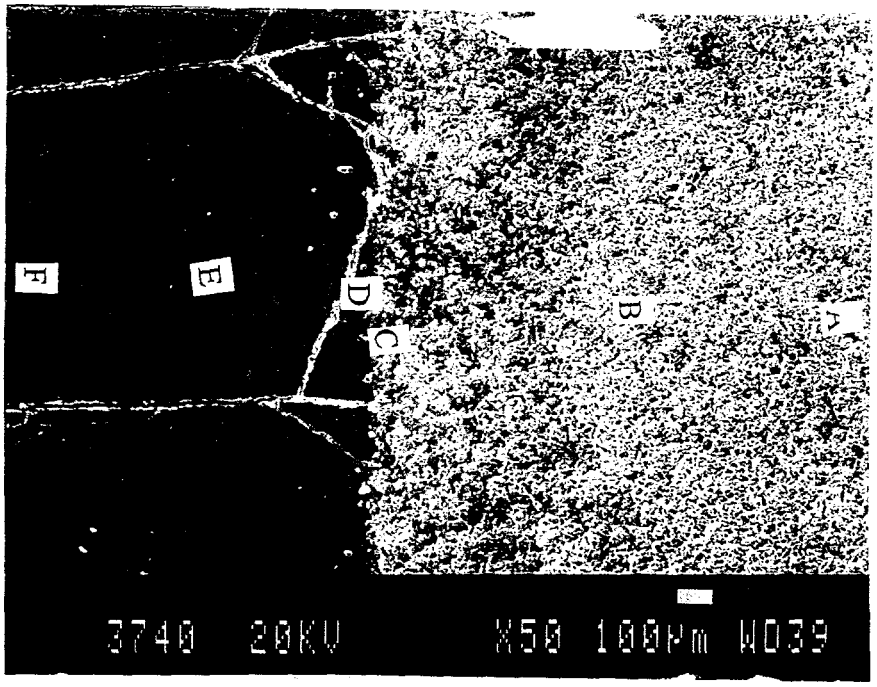

Figure 18. Mullite/Aluminum Titanate Slag Boundary

Table 8. Summary of $3Al_2O_3 \cdot 2SiO_2/Al_2TiO_5$ Analysis

Atomic % (SSQ)						
Area	**Al**	**Ti**	**Si**	**Ca**	**K**	**Fe**
A	53	29	17	1	0	0
B	50	28	19	2	<1	1
C	51	21	18	1	0	9
D	24	4	56	6	2	9
E	45	1	43	2	<1	8
F	27	1	55	6	1	9

Aluminum Titanate/Alumina - Al_2TiO_5/Al_2O_3

With the excellent slag resistance of Al_2O_3, 30 weight percent of Al_2TiO_5 was added to reduce its CTE mismatch with SiC. The Al_2TiO_5/ Al_2O_3 sample after exposure is shown in Figure 19. Except for a light coating of slag, visual examination showed no changes to the sample The region of the sample examined via SEM and EDS is shown in Figure 20, with the EDS results presented in Table 9. Regions A and B show typical intensities for the baseline material. When Area C was inspected by SEM, both a dark and a light phase were seen (the left side of Figure 21). EDS analysis of the dark (C_d) and light (C_l) phases was performed. The dark phase in this area had Si and Fe present, while the light phase was rich in Ti (compared to Areas A and B) and also had Fe. This would indicate that the light phase is the titanate which, as we have seen before, had Fe substitute into the structure for Al. The dark phase is some form of reaction product of Al_2O_3 with the slag. Area D was immediately adjacent to the sample boundary in the slag. Block-shaped precipitates (not the bright white precipitates common to the slag) were visible in this region (Figure 22) and showed (D_p) very high Fe and Si levels, but also contained significant Al and Ca levels. These precipitates also preferentially contained Ti. The matrix in this region (D_m) had a composition somewhat off from the bulk slag (Area E) in Fe and Al, though the differences are minor.

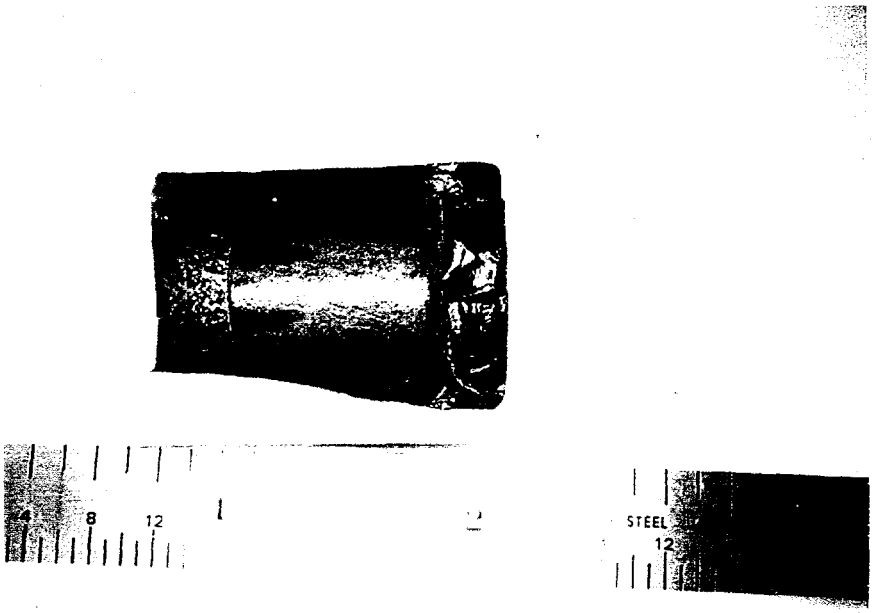

Figure 19. Macro View of Al_2TiO_5/Al_2O_3 Sample After Exposure

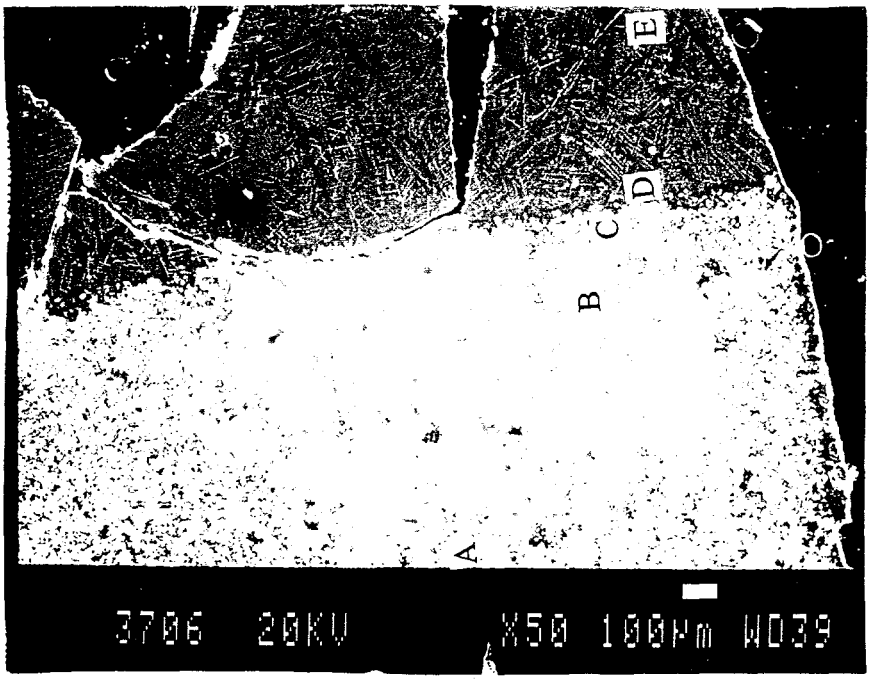

Figure 20. Boundary Region of Al_2TiO_5/Al_2O_3

Table 9. Summary of EDS Results for Al_2TiO_5/Al_2O_3

	Intensity					
Area	**Al**	**Ti**	**Si**	**Ca**	**K**	**Fe**
A	.51	.06	.00	.00	.00	.00
B	.51	.06	.00	.00	.00	.00
C_d	.70	.16	.19	.00	.00	.06
C_l	.58	.34	.00	.00	.00	.10
D_p	.41	.12	.74	.13	.05	.71
D_m	.29	.00	.71	.13	.02	.05
E	.35	.01	.73	.11	.02	.09

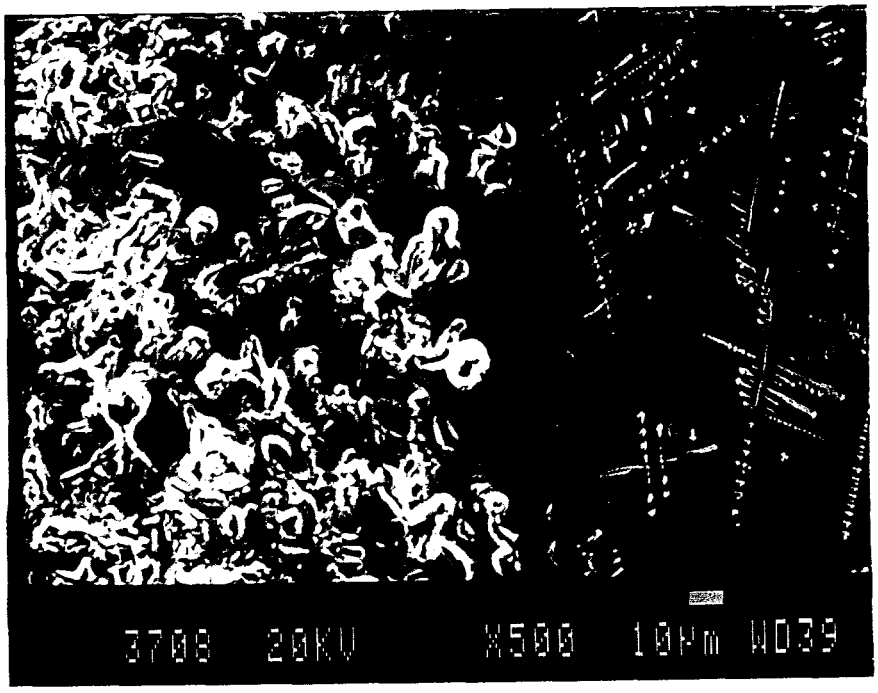

Figure 21. Al_2TiO_5/Al_2O_3 - Slag Boundary Showing Two Phases in Sample

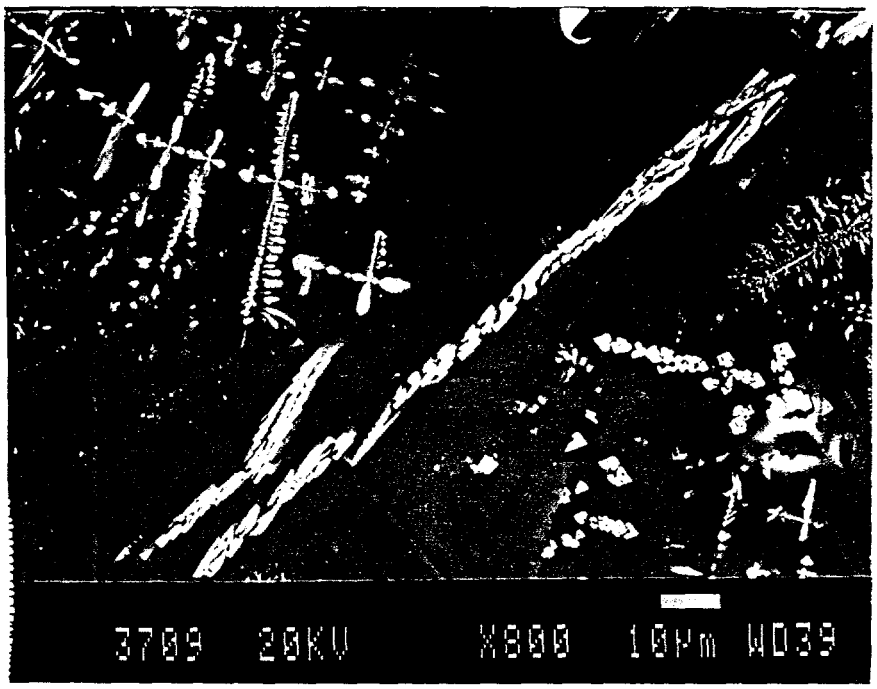

Figure 22. Slag Adjacent to Al_2TiO_5/Al_2O_3 Showing Block-Shaped Precipitates

Barium Zirconate - $BaZrO_3$

Barium zirconate was selected for its potential to resist reaction with silica, the major component in the slag. The $BaZrO_3$ pellet is shown in Figure 23 after exposure, and did not display any evidence of reaction with the slag. A typical area of the sample (Figure 24) was examined by EDS with the results summarized in Table 1-. The sharp boundary between the $BaZrO_3$ and the slag is immediately noticed in Figure 24. Examining Areas A, B, and C revealed only Ba and Zr present in the sample, even within 20 µm of the slag boundary (Area C). However, the slag adjacent to the $BaZrO_3$ (Figure 25) had obvious precipitates, which were determined (D_p) to contain only Zr. The slag matrix in Area D had a high level of Ba, as well as typical intensities for the base slag material. Throughout the balance of the slag (Areas E, F, and G), Ba is present in large amounts, and Zr is present for at least 0.8 mm into the slag (Area F). These results indicate that Ba is removed from $BaZrO_3$ at a substantial rate, with the remaining Zr forming the precipitates. The sharp boundary between the slag and the $BaZrO_3$ is a result of the chemical etching of the sample.

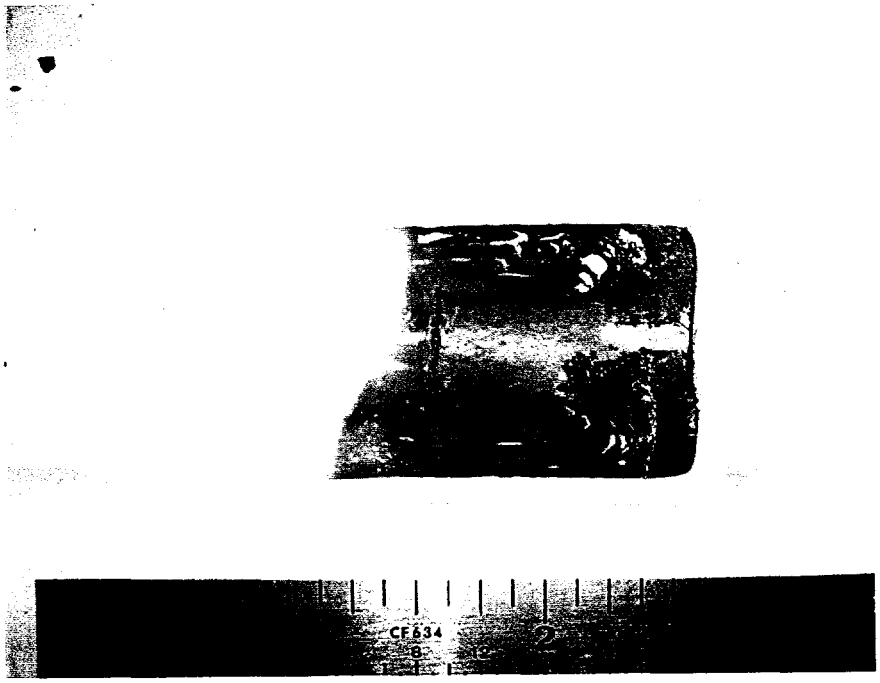

Figure 23. $BaZrO_3$ After Slag Exposure

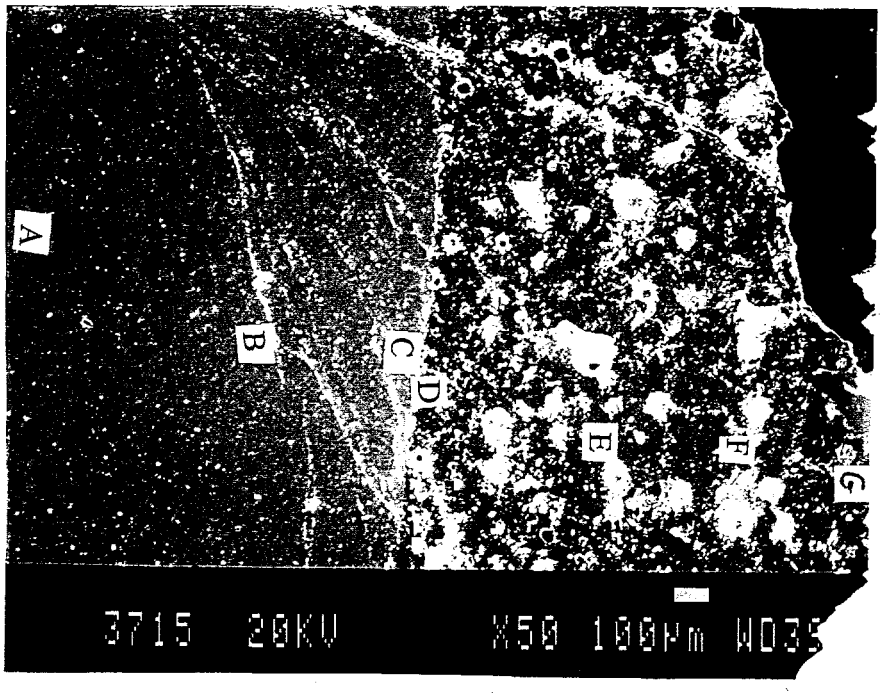

Figure 24. $BaZrO_3$ - Slag Boundary with EDS Locations

Table 10. Summary of EDS Results for $BaZrO_3$

	Intensity						
Area	**Ba**	**Zr**	**Al**	**Si**	**K**	**Ca**	**Fe**
A	.79	.60	.00	.06	.00	.00	.00
B	.79	.63	.00	.00	.00	.00	.00
C	.79	.63	.00	.00	.00	.00	.00
D_p	.00	.94	.00	.00	.00	.00	.00
D_m	.81	.05	.31	.81	.00	.14	.15
E	.38	.75	.21	.63	.00	.10	.10
F	.59	.51	.29	.60	.00	.10	.12
G	.48	.00	.55	.75	.05	.05	.06

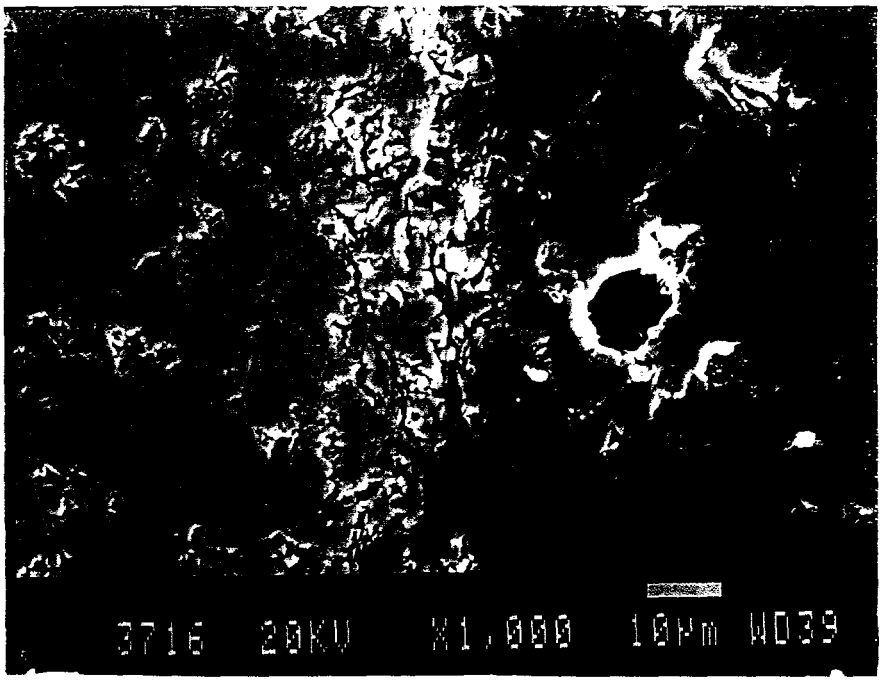

Figure 25. Precipitates at $BaZrO_3$ - Slag Interface

Magnesium Chromite - $MgCr_2O_4$

Magnesium chromite ($MgCr_2O_4$) is a common refractory material for glass processing and it may be resistant to formation of silicates. The $MgCr_2O_4$ sample after exposure is shown in Figure

26. The sample has been complete encased in slag and is difficult to see in the figure. The region of the sample examined by EDS is shown in Figure 27 with the analytical results summarized in Table 11. The composition of the $MgCr_2O_4$ is uniform at Areas A, B, and C, with only trace levels (atomic percent) of Si and Fe. Examining the boundary region more closely (Figure 28) revealed the formation of two reaction layers (Areas E. and F, respectively). The $MgCr_2O_4$ very near to these reaction layers (Area D) is consistent with the interior of the sample, although a small decrease in Mg is seen as well as higher, but still minor, amounts of Si and Fe. The inner reaction layer (Are E) may be consistent with a Cr-Al-Fe solid solution, since all three oxides are isomorphic. Region F, and outer reaction layer, is Al rich with significant amounts of Fe and Cr. Precipitates in the slag (Figure 28) have the same composition as Area F. The composition of the slag away from the $MgCr_2O_4$ (Area G) is representative of the base slag.

Figure 26. $MgCr_2O_4$ Samples After Exposure

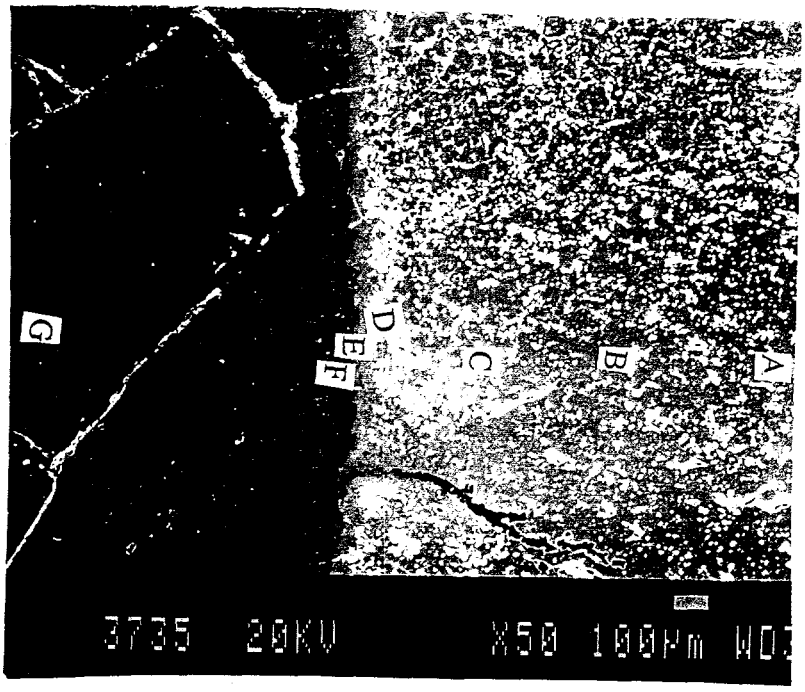

Figure 27. $MgCr_2O_4$ - Slag Boundary with EDS Locations

Table 11. Summary of EDS Results for $MgCr_2O_4$

Atomic % (SSQ)							
Area	**Al**	**Si**	**Ca**	**K**	**Fe**	**Mg**	**Cr**
A	.00	.02	.00	.00	.01	.26	.71
B	.00	.02	.00	.00	.00	.27	.71
C	.00	.03	.00	.00	.03	.22	.72
D	.00	.04	.00	.00	.03	.19	.74
E	.06	.03	.00	.00	.18	.00	.73
F	.77	.00	.00	.00	.12	.00	.11
G	.28	.48	.09	.02	.09	.06	.00

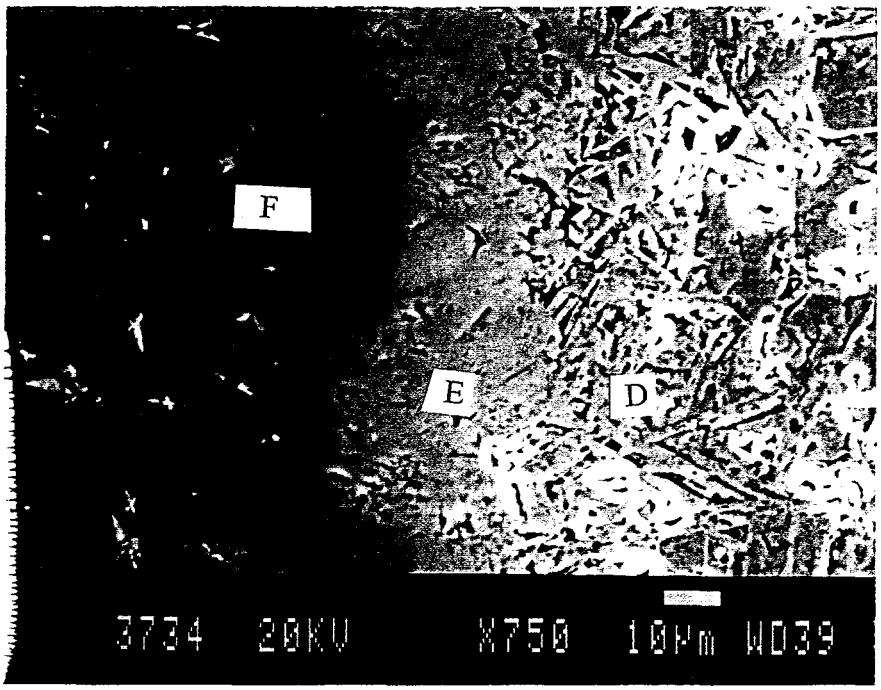

Figure 28. Dual Reaction Layer on $MgCr_2O_4$

Yttrium Chromite - $YCrO_3$

Yttrium Chromite ($YCrO_3$) was selected for its potential to resist formation of silicates. The $YCrO_3$ pellet is shown after exposure in Figure 29. The limited visual inspection of the pellet, which was inhibited by the slag covering much of the sample, did not reveal any dramatic change in the sample shape. Figure 30 is an overview of the $YCrO_3$ - slag region inspected by EDS (Table 12). This figure clearly shows extensive reaction between the slag and the $YCrO_3$, with a large amount of precipitates in the slag and a rounding of the edge of the $YCrO_3$ pellet. As shown in Table 12, Cr is present in the slag even in Area A which is approximately 400 µm from the apparent edge of the $YCrO_3$. Although no precipitates are visible in Area B, the Cr content has increased significantly. Area C is the boundary for precipitate formation, and analysis on one of the particle (C_p) gives a Cr-Al-Fe composition, with Cr the dominant species. In contrast, the slag matrix in the area (C_m) is typical of the base slag, except for a small amount of Cr. This pattern is continued in Areas D and E, though the analysis shown in Table 12 does not separate out the matrix and precipitate portions. In Areas F, G, and H, the presence of only Y and Cr demonstrates that the slag is not penetrating the $YCrO_3$, but that the $YCrO_3$ is being dissolved by the slag. It is also apparent that the stoichiometry of the $YCrO_3$ may not be correct as shown by these intensity values. Although it is not clear in Figure 30, Area I was much "brighter" than other regions of the $YCrO_3$, which often indicates a higher average atomic number for that material. EDS analysis of this area did show a Cr to Y intensity that would be more in-line with a stoichiometric material (note: the correction factors for Y and Cr are approximately 1.36 and 1.04, respectively). However, Area J also contains precipitates and a small area analysis shows the major components of the slag with Y and Cr.

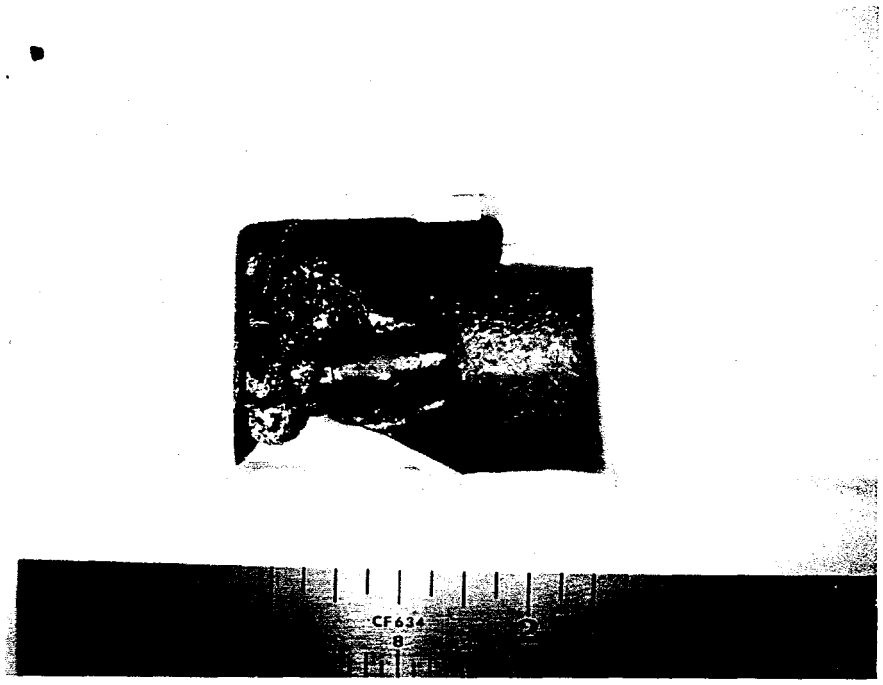

Figure 29. $YCrO_3$ Pellet After Exposure

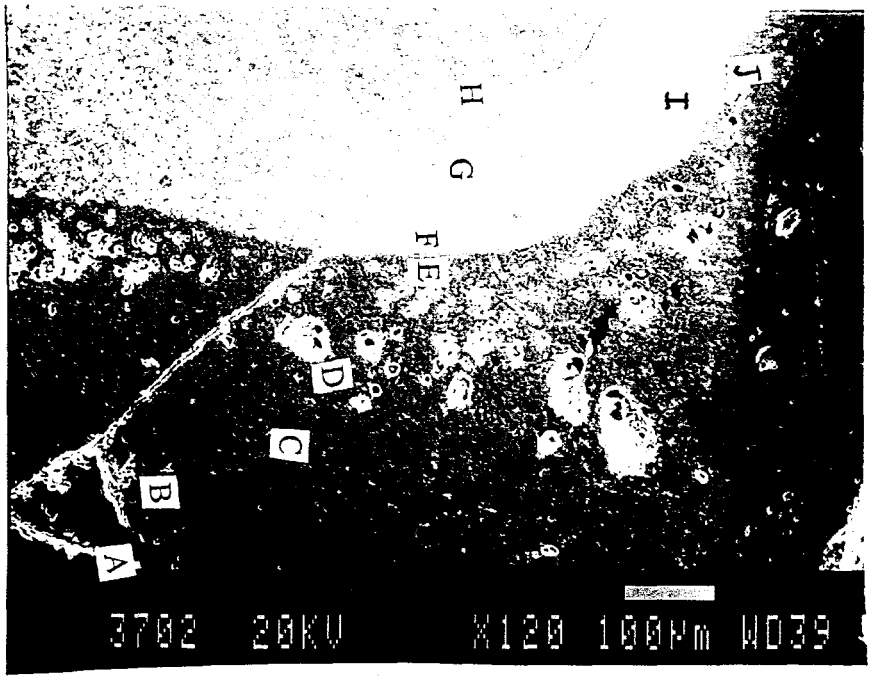

Figure 30. $YCrO_3$ - Slag Region Showing EDS Locations

Table 12. Summary of EDS Analysis for $YCrO_3$

	Intensity					
Area	**Al**	**Si**	**Ca**	**Fe**	**Cr**	**Y**
A	.47	.88	.13	.09	.09	.00
B	.53	.91	.13	.13	.19	.00
C_d	.31	.00	.00	.23	.91	.00
C_m	.25	.56	.08	.05	.03	.00
D	.38	.20	.03	.19	.79	.00
E	.28	.23	.03	.16	.81	.00
F	.00	.00	.00	.00	.91	.40
G	.00	.00	.00	.00	.81	.44
H	.00	.00	.00	.00	.88	.46
I	.00	.00	.00	.00	.60	.60
J	.25	.39	.00	.09	.53	.20

NZP-Type (CS-50)

Sodium Zirconium Phosphate (NZP) materials have low CTEs and have been shown to be corrosion resistant in some applications. For this study, a calcium strontium phosphate variant was selected after discussions with Stinton and Natesan of Oak Ridge and Argonne National Laboratories, respectively. The calcium strontium phosphate was provided by LoTec and designated CS-50. The CS-50 sample is shown after exposure in Figure 31. Examination of the top surface reveals a dark ring approximately 1.6 mm thick around the entire edge of the CS-50. A portion of this ring spalled away from the bulk of the sample during its removal from the crucible. The appearance of this ring suggests that the CS-50 had reacted strongly with the slag during the exposure tests. The comparative XRD patterns for CS-50 (with the as-received sample shown on the bottom) shows distinct shifts in the peaks, which indicate a significant change in composition. After metallographic preparation of the sample, the extent of the reaction between the slag and the CS-50 is obvious (Figure 32), with the sample exhibiting a "Flame" structure. The "tip" of the sample, where the original diameter of the sample is obvious reduced, was immersed in the slag. The symmetric patterns of composition and cracks is strongly indicative of a diffusion controlled reaction. Approximately 70 percent of the original sample has undergone some visible change during the 100 hour test. Figure 33 shows the region of the CS-50 examined by EDS as well as the locations of the analysis points. The results of the analysis are presented in Table 13. Area 1 of the sample is in the "core" of the sample and shows only the expected elements for the CS-50. Given the overlap of the P and Zr peaks, we could not resolve these materials via EDS and they are listed together in the analysis. In Areas 2, 3, and 4, which exhibited extensive void formation, the sample has a significant level of Al, and in Area 4 an increase amount of Zr/P. Area 5 (Figure 34) is in the slag and consisted of a matrix (5_m) and precipitate (5_p). The matrix is consistent with the base slag composition, while the precipitate consisted of only Zr/P and Si. The relatively consistent levels of Sr and Ca in the reaction layer

of the S-50, progress of Al and the formation of Zr/P - based precipitates, indicates an exchange of Al for Zr/P. The resulting change in physical properties with this substitution could account for structural changes in the sample.

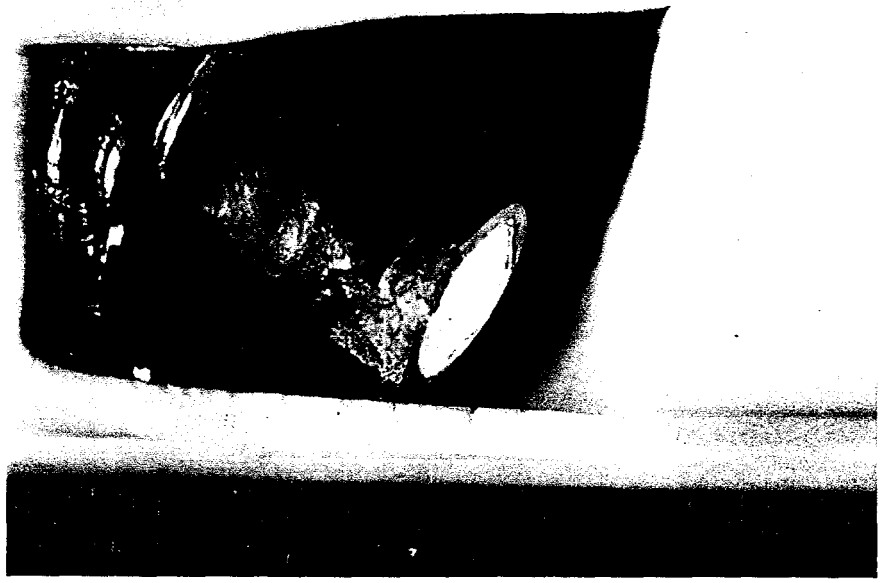

Figure 31. CS-50 Sample After Exposure

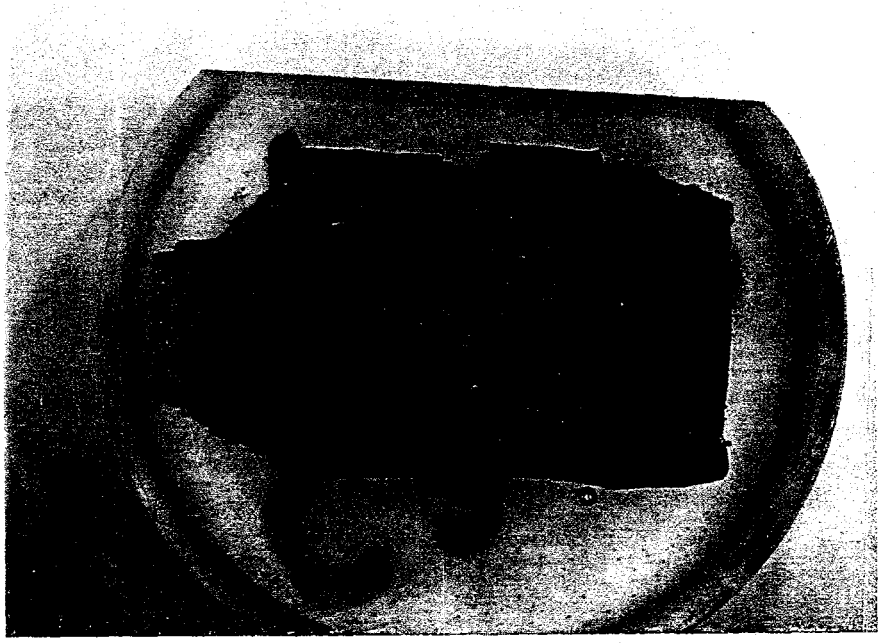

Figure 32. Optical Micrograph of Reaction Zones in CS-50

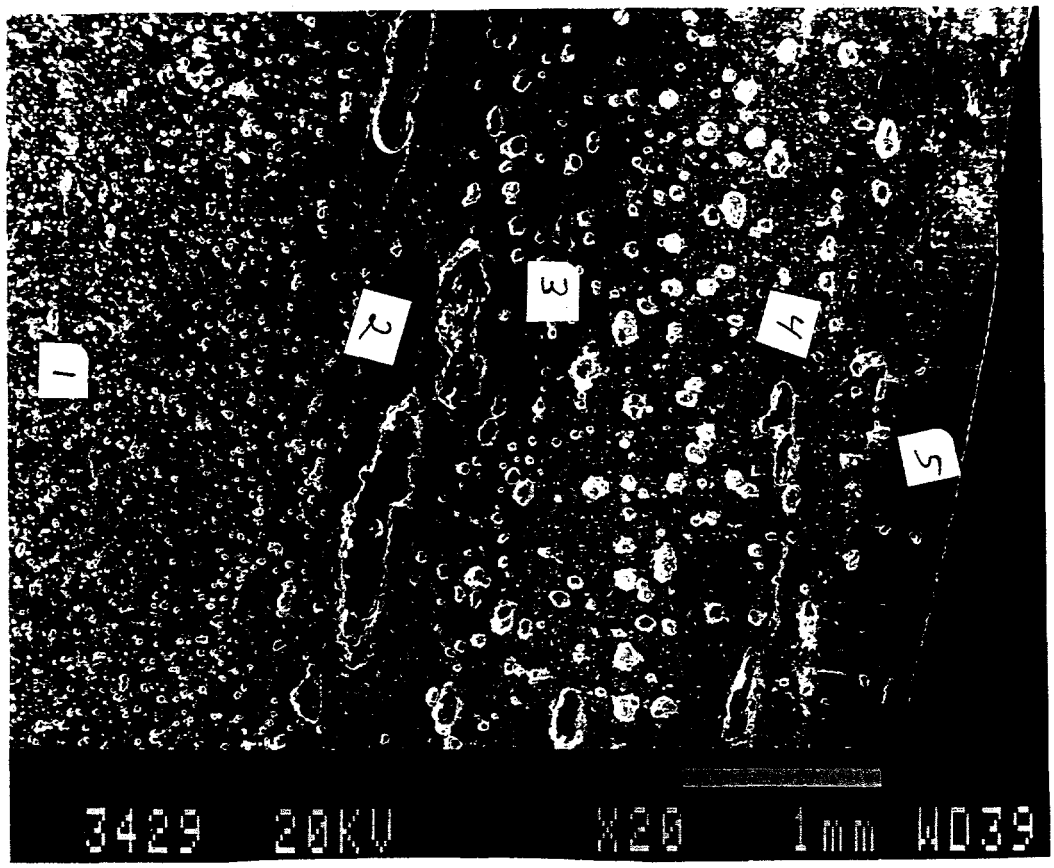

Figure 33. CS-50 - Slag Region Examined by EDS

Table 13. Summary of EDS Results for CS-50

	Intensity						
Area	**Sr**	**Zr/P**	**Al**	**Si**	**K**	**Ca**	**Fe**
1	.31	.66	.00	.00	.00	.08	.02
2	.25	.50	.18	.00	.00	.13	.03
3	.28	.52	.16	.00	.00	.08	.02
4	.33	.63	.18	.00	.00	.10	.03
5_m	.00	.05	.21	.63	.03	.05	.05
5_p	.00	.44	.00	.63	.00	.00	.00

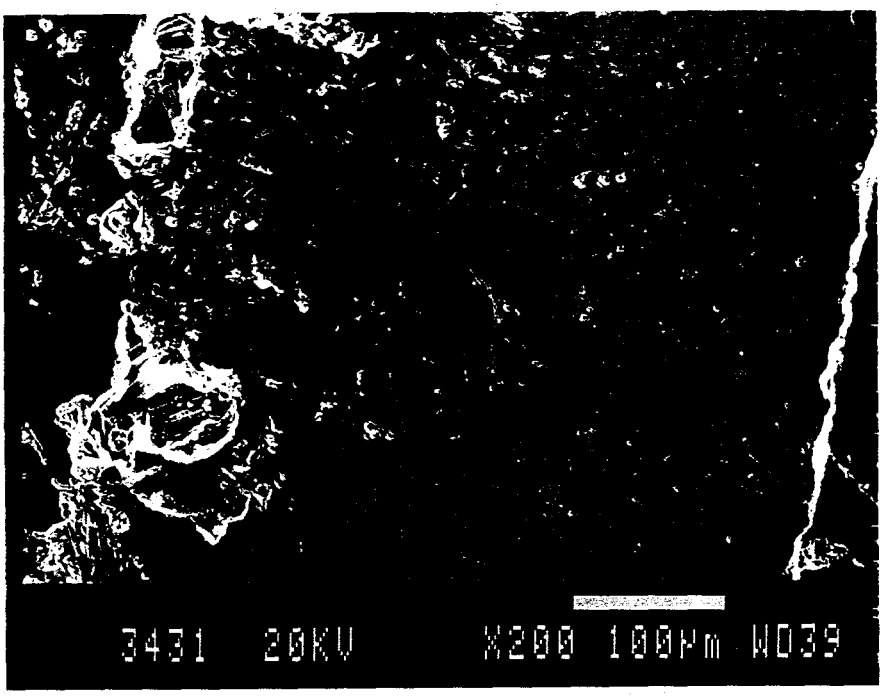

Figure 34. Area 5 of CS-50 Sample Showing Precipitates in Slag

Zirconium Titanate - $ZrTiO_4$

The CTE of zirconium titanate ($ZrTiO_4$) is a good match for SiC, and it was selected for this property as well as its potential to resist attack by silica. The $ZrTiO_4$ sample is shown in Figure 35 after exposure to the ash. The ash wet the sample and during its removal from the crucible several small sections of the ash fracture and pulled away some of the $ZrTiO_4$. XRD of the sample did not show any new phases, and the only apparent change being an increase in the definition of the diffraction peaks. An overview of the part of the sample analyzed by EDS is shown in Figure 36, with the EDS results summarized in Table 14. Area A was found to be consistent with the typical slag composition. It can clearly be seen in Figure 37 that large precipitates had formed near the $ZrTiO_4$ interface. When analyzed, they were found to consist of Zr and Si only. The slag matrix between these particles was somewhat depleted in Si and higher in Ti. Adjacent to the $ZrTiO_4$, the precipitates were of different composition (C_{light}), which indicates that the $ZrTiO_4$ is being dissolved by the slag with the elements diffusing into the bulk slag where the Zr-Si precipitates form and Ti remains in solution in the slag. Within the $ZrTiO_4$ sample (Areas D, E, and F), two phases were found. The dominant (light) phase, seen in Figure 38, is $ZrTiO_4$, while the dark phase shows a modified slag composition. In addition to the basic slag materials, significant amounts of both Zr and Ti are present in areas D and E. Little Ti and no Zr were detected in the slag in Area F.

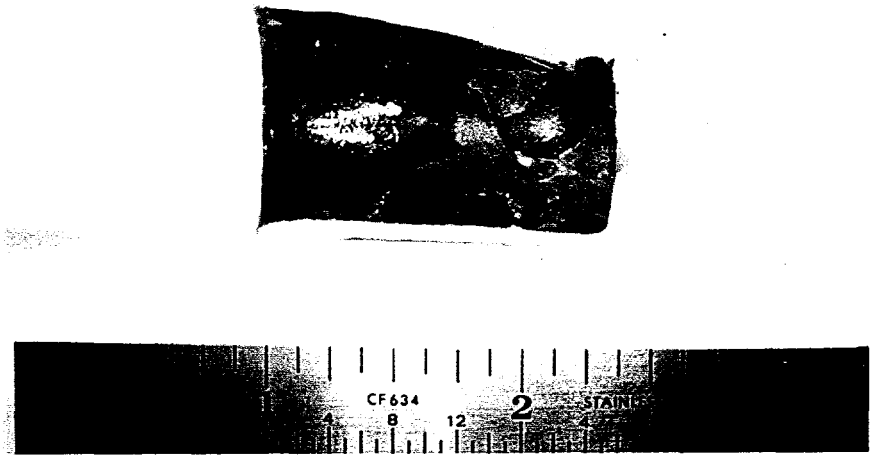

Figure 35. $ZrTiO_4$ Sample After Exposure

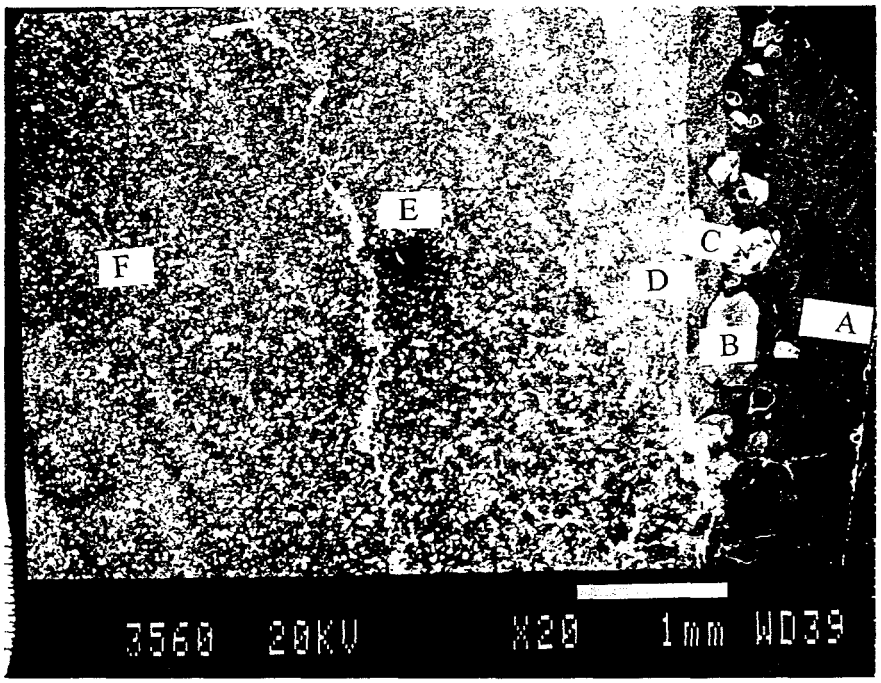

Figure 36. $ZrTiO_4$ - Slag Analysis Region

Table 14. Summary of EDS Analysis for $ZrTiO_4$

	Intensity						
Area	**Zr**	**Ti**	**Al**	**Si**	**K**	**Ca**	**Fe**
A	.00	.05	.35	.75	.04	.05	.03
B - ppt	.40	.00	.00	.63	.00	.00	.00
C - light	.91	.10	<.05	.00	.00	.00	.00
D - light	.94	.90	.00	.00	.00	.00	.00
D - dark	.14	.19	.28	.84	.05	.13	.00
E	.60	.48	.35	.45	.02	.05	.02
F - dark	.00	.04	.38	.94	.05	.16	.04
F - light	.56	.46	.00	.00	.00	.00	.00

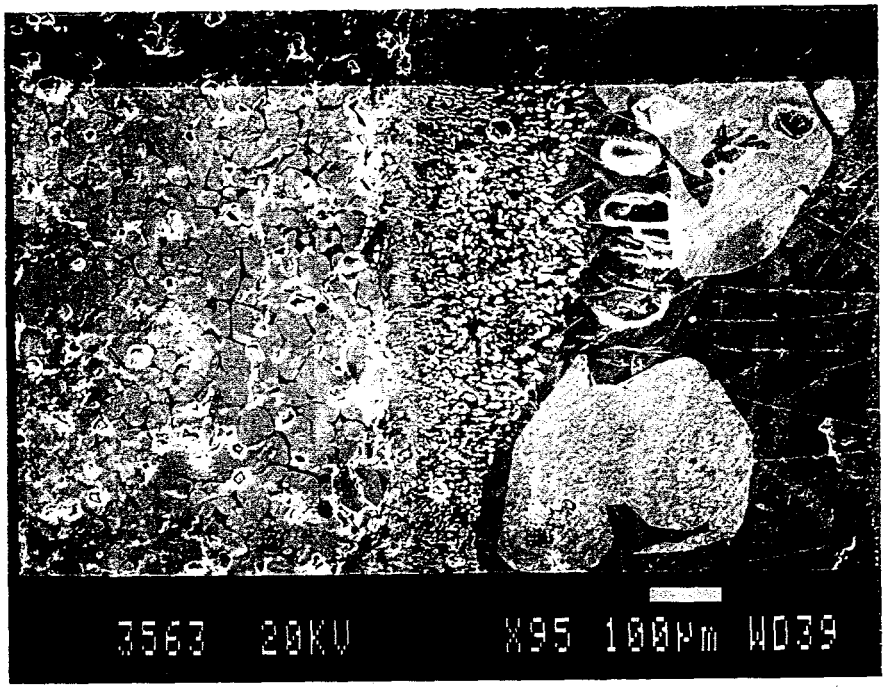

Figure 37. $ZrTiO_4$ - Slag Interface Showing Large (Area B) & Small (Area C) Precipitates

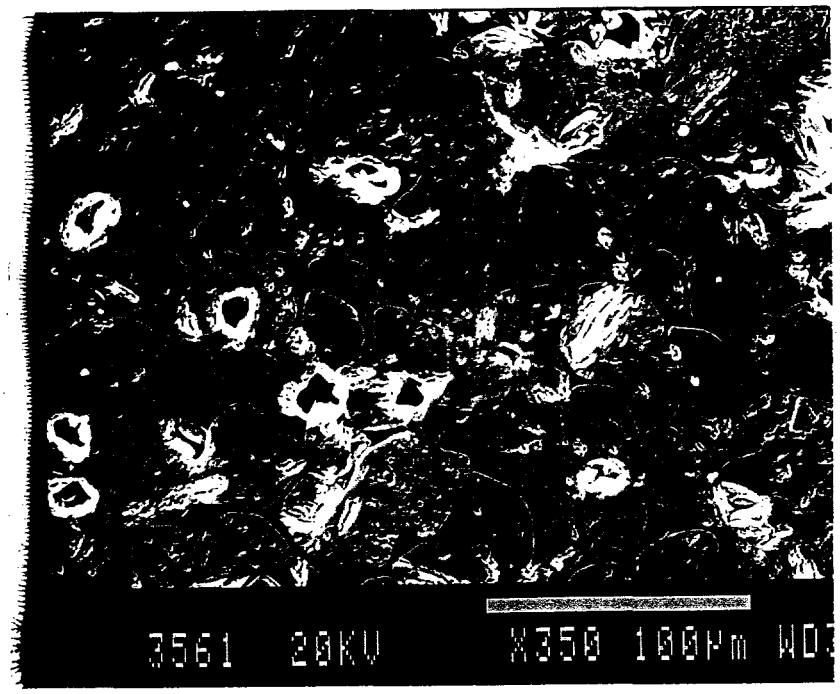

Figure 38. Interior of Sample Showing $ZrTiO_4$ (light) and Slag (dark)

5.0 SUMMARY AND CONCLUSIONS

The results of this corrosion screening effort can be summarized as follows:

1. Good agreement with other researchers for the behavior of the baseline materials (reaction bonded SiC, sintered α-SiC, and Al_2O_3) in the slag was obtained.

2. Mullites, RBAO (SiC_p/ Al_2O_3), Al_2TiO_5, Mullite/ Al_2TiO_5, and Al_2TiO_5/Al_2O_3 all appear to be potentially viable protective coatings for SiC heat exchanger tubes in coal slag environments. In all cases, the slag components were detected only in the near surface region (typically 20 μm or less).

3. $MgCr_2O_4$ forms a double reaction layer, Al_2O_3-based on the exterior and Cr_2O_3-based on the interior, which may prove to provide a stable barrier coating to the slag.

4. $YCrO_3$, $ZrTiO_4$, and $BaZrO_3$ all undergo a dissolution reaction with the slag and form precipitates in the slag. Except for the precipitates, no other gross changes were seen in these samples.

5. The CS-50 sample (calcium strontium zirconium phosphate version of NZP) undergoes dramatic morphological changes, including the formation of large pores/cracks, that are indicative of a diffusion control reaction with the slag. Large precipitates, consisting of either Zr-Si or P-Si, were found in the slag adjacent to the CS-50 sample.

6. $CaTiO_3$ underwent a catastrophic reaction with the slag that resulted in the destruction of the Al_2O_3 crucible as well as the sample.

7. The results of these tests cannot be used to project coating life for any of the potentially useful coatings because only a single exposure time was used, which prevented determination of reaction rate information, and a finite amount of slag was available for interaction with each sample.

8. This effort demonstrated a simple and useful method for screening a wide range of candidate protective coating materials.

The following recommendations are made based upon the results of this study:

- Additional testing of successful candidates must be done, with an emphasis on determining reaction rate data, and measuring the hot hardness of the most promising materials.

- Candidate materials should also undergo exposure to other slag compositions to test the breadth of their resistance to acidic and basic slags.

- Candidate coatings should be tested for thermochemical stability with SiC in an oxidizing environment, and their thermal shock and thermal fatigue resistance as a coating on SiC.

- Once reaction rate data is available, candidate coatings should be applied to SiC tubular substrates for exposure to simulated coal combustion environments. This testing should include the continuous/semi-continuous introduction of slag to the specimens.

- After exposure, coated-SiC tubes should be tested for retained strength and examined for interaction between the three components (substrate-coating-slag).

- Once a material has successfully passed these tests, long term testing on sub-scale components will be required before its integration into an advanced coal-fired power system.

6.0 REFERENCES

1 N. J. Orozco, *High-Pressure Ceramic Air Heater for Indirectly Fired Gas Turbine Application*, **Proceedings of the Joint Contractors Meeting: FE/EE Advanced Turbine Systems Conference FE Fuel Cells and Coal -Fired Heat Engines Conference**, Donald W. Geiling, ed., U. S. Department of Energy, Office of Fossil Energy, METC, August 3-5, 1993

2 N. J. Orozco, P. G. LaHaye, J. Strom-Olsen, J. L. Seger, and H. Pickup, *Externally Fired Combined Cycle Demonstration* **Proceedings of the Advanced Coal-Fired Power Systems '95 Review Meeting - Volume 1**, Heather M. McDaniel, Darren J. Mollot, and Venkat K. Venkataraman, eds., U. S. Department of Energy, Office of Fossil Energy, METC, June 27-29, 1995

3 H. Pickup, personnel communication, December 1994

4 N. S. Jacobson, "Corrosion of Silicon-Based Ceramics in Combustion Environments", J. Am. Ceram. Soc. **76** [1] 3-28 (1993)

5 T. M. Strobel, J. P. Hurley, K. Breder, and J. E. Holowczak, *Coal-Slag Corrosion and Strength Degradation of Siliconized Silicon Carbide* **Proceedings of the 19th Annual Cocoa Beach Conference & Exposition on Composites, Advanced Ceramics, Materials, and Structuers**, The American Ceramic Society, January 8-12, 1995.

6 N. S. Jacobson, and J. L. Smialek, "Burner Rig Corrosion of SiC at 1,000oC", NASA-Lewis Research Center Report TM-87061

7 K. Natesan, M. Yanes-Herrero, and C. Fornasieri, "Corrosion Performance of Materials for Advanced Combustion Systems" Argonne National Laboratory Report ANL/FE-93/1

8 G. R. Pickrell, T. Sun, and J. J. Brown, "High Tempeture Alkali Corrosion of Ceramics", Quarterly Report #2 for Contract DE-FG22-91PC91309, U. S. Department of Energy, PETC

9 T. M. Strobel, J. P. Hurley, C. L. Senior, and J. E. Holowczak, "Coal Slag Corrosion of Silicon Carbide-Based Ceramics in a Combustion Environment" in **Silicon-Based Structural Ceramics**, Brian W. Sheldon and Stephen C. Danforth, eds., Ceramic Transations **42**, The American Ceramic Society

10 C. L. Senior, G. A. Moniz, J. P. Hurley, and T. M. Strobel, "Corrosion of Silicon Carbides by Ash and Vapor in a Coal Combustion Environment", in **Silicon-Based**

Structural Ceramics, Brian W. Sheldon and Stephen C. Danforth, eds., Ceramic Transations **42**, The American Ceramic Society

11 T. M. Strobel, J. P. Hurley, K. Breder, and J. E. Holowczak, "Coal Slag Corrosion and Strength Degradation of Silicon Carbide/Alumina Composites" Cer. Eng. Sci. Proc. **15** [9] pg 579-586 1994

12 W. Boss, "High Performance Materials in Coal Conversion Utilization" presented at U. S. Department of Energy peer review of AR&TD projects, Oak Ridge National Laboratory, February 28 to March 2, 1995

13 J. P. Hurley, *Factors Effecting the Corrosion Rates of Ceramics in Coal Combustion Systems* **Proceeding of the Ninth Annual Conference of Fossil Energy Materials**, N. C. Cole and R. D Judkins, eds., U. S. Department of Energy, Fossile Energy Ar&TD Materials Program, Oak Ridge National Laboratory, May 16-18, 1995

14 S. Wu and N. Claussen, "Reaction Bonding and Mechanical Properties of Mullite/Silicon Carbide Composites", J. Am. Ceram. Soc., **77** [11] 2898-904 (1994)

15 S. S. Manoharan and K. C. Patil, "Combustion Synthesis of Metal Chromite Powders", J. Am. Ceram. Soc., **75** [4] 1012-15 (1992)